Georgia Southern University
Digital Commons@Georgia Southern

Electronic Theses and Dissertations | Graduate Studies, Jack N. Averitt College of

Spring 2015

Smart Distributed Generation Systems Using Improved Islanding Detection and Event Classification

Bikiran Guha

Follow this and additional works at: https://digitalcommons.georgiasouthern.edu/etd

Part of the Power and Energy Commons

Recommended Citation
Guha, Bikiran, "Smart Distributed Generation Systems Using Improved Islanding Detection and Event Classification" (2015). *Electronic Theses and Dissertations*. 1262.
https://digitalcommons.georgiasouthern.edu/etd/1262

This thesis (open access) is brought to you for free and open access by the Graduate Studies, Jack N. Averitt College of at Digital Commons@Georgia Southern. It has been accepted for inclusion in Electronic Theses and Dissertations by an authorized administrator of Digital Commons@Georgia Southern. For more information, please contact digitalcommons@georgiasouthern.edu.

SMART DISTRIBUTED GENERATION SYSTEMS USING IMPROVED ISLANDING DETECTION AND EVENT CLASSIFICATION

by

BIKIRAN GUHA

(Under the Direction of Rami Haddad)

ABSTRACT

Distributed Generation (DG) sources have become an integral part of modern decentralized power systems. However, the interconnection of DG systems to the power grid can present several operational challenges. One such major challenge is islanding detection. Islanding occurs when a DG system is disconnected from the rest of the power grid. Islanding can present serious safety hazards and therefore an accurate and fast islanding detection technique is mandated by DG interconnection standards such as IEEE 1547 and UL 1741. Conventional islanding detection techniques passively monitor the local power system parameters such as voltage and frequency to detect islanding. These techniques have large non-detection zones and are prone to nuisance tripping. Therefore, two improved and computationally inexpensive passive islanding detection techniques for inverter-based DG systems were proposed. The techniques monitor the ripple content in the rate of change of frequency and voltage amplitude waveforms using time domain-spectral analysis. The proposed techniques were tested for inverter-based DG systems modeled according to IEEE 929-2000 standard. Results indicated that both techniques were not only capable of detecting islanding, but also able to accurately distinguish between islanding and non-islanding events under a wide range of operating conditions. Furthermore, a novel Smart DG system which is able to detect and classify events was proposed. This added intelligence has considerable impact on the safety and operation of such DG systems. This feature will help the system operator develop a clear understanding of the operating requirements needed to mitigate the effects of such events. The event classification technique has been implemented using artificial neural networks (ANN) with a set of local input parameters. Five parallel ANNs have been designed with a majority vote final stage to represent the final classification output. A total of 310 event cases have been generated to test the performance of the technique. This technique classified the events within 10 cycles of their occurrence with a 98% average classification accuracy.

INDEX WORDS— Passive islanding detection, Smart grid, Anti-islanding, Voltage RMS, Rate of change of frequency, Distributed generation, Event classification, Artificial Neural Networks

SMART DISTRIBUTED GENERATION SYSTEMS USING IMPROVED ISLANDING DETECTION AND EVENT CLASSIFICATION

by

BIKIRAN GUHA

B. Tech. Electrical Engineering, West Bengal University of Technology, India, 2013

A Thesis Submitted to the Graduate Faculty of Georgia Southern University in Partial Fulfillment of the Requirements for the Degree

MASTER OF SCIENCE IN APPLIED ENGINEERING

STATESBORO, GEORGIA

© 2015

BIKIRAN GUHA

All Rights Reserved

SMART DISTRIBUTED GENERATION SYSTEMS USING IMPROVED ISLANDING DETECTION AND EVENT CLASSIFICATION

by

BIKIRAN GUHA

Major Professor:	Rami Haddad
Committee:	Youakim Kalaani
	Frank Goforth
	Adel El-Shahat

Electronic Version Approved:
May 2015

ACKNOWLEDGMENTS

I would like to express my deepest gratitude to my advisor and committee chair Dr. Rami Haddad for his full support, expert guidance, understanding and encouragement throughout my study and research. Without his unending patience, timely wisdom and counsel, this thesis work would not have been possible. I would also like to thank my committee members, Dr. Youakim Kalaani, Dr. Adel El-Shahat and Dr. Frank Goforth for their expert advice and support.

Finally, I would like to thank my family and friends for their continued love and support in every aspect of my life.

Table of Contents

ACKNOWLEDGMENTS **iv**

LIST OF FIGURES **v**

LIST OF TABLES **vii**

1 INTRODUCTION **1**

Islanding Detection 2

Event Classification 4

2 LITERATURE REVIEW **6**

Islanding Detection Standards and Non Detection Zones 6

Passive Islanding Detection Techniques 7

Active Islanding Detection Techniques 12

Hybrid Islanding Detection Techniques 17

Machine Learning-based Detection Techniques 18

Remote Islanding Detection Techniques 22

Comparative Analysis of Existing Islanding Detection Techniques 24

Power Quality Event Detection and Classification 25

3 TECHNICAL DETAILS OF THE PROPOSED TECHNIQUES **29**

Voltage Amplitude based Islanding Detection 29

Rate of Change of Frequency based Islanding Detection 36

DG Event classification using Artificial Neural Networks 38

4 RESULTS AND PERFORMANCE ANALYSIS **44**

Results of Voltage Amplitude based Islanding Detection Technique 45

Results of ROCOF based Islanding Detection Technique 52

Results of ANN-based DG Event Classification Technique 55

5 CONCLUSIONS AND FUTURE WORK **61**

Bibliography **63**

List of Figures

Figure 1 A typical islanding scenario 2

Figure 2 Taxonomy of islanding detection techniques 3

Figure 3 NDZ representation of (a) passive and active techniques in active/reactive power mismatch domain (b) active techniques in frequency-Q_f domain 7

Figure 4 Types of popular passive techniques 8

Figure 5 A typical system model of a grid-connected DG source 9

Figure 6 Phase shift during islanding 10

Figure 7 Harmonic current flow in an inverter based system for (a) grid-connected and (b) islanded conditions 12

Figure 8 Taxonomy of active detection techniques 13

Figure 9 Equivalent impedance seen by the DG during (a) grid-connected and (b) islanded conditions 13

Figure 10 PCC voltage and output current waveform of an inverter applying active frequency drift 16

Figure 11 Common types of machine learning based detection techniques 18

Figure 12 Taxonomy of remote islanding detection techniques 22

Figure 13 Output power of DG inverter 29

Figure 14 Root Mean Square (RMS) of single phase voltage waveforms at PCC for a) Grid-connected condition, b) islanding condition, c) three phase short circuit fault condition 30

Figure 15 Proposed islanding detection technique block diagram 30

Figure 16 Waveforms of all the stages of the islanding detection technique 31

Figure 17 Islanding detection waveform. a) Grid-connected condition, b) islanding condition, c) three phase short circuit fault condition 32

Figure 18 Algorithm for the detection technique 33

Figure 19 Effect of changing the fundamental frequency of (a) the Mean 3 block and (b) the RMS block on islanding detection waveform output 34

Figure 20 Effect of combined changing of the fundamental frequencies of the Mean 3 and RMS block on islanding detection waveform output 34

Figure 21 Effect of combined changing of the fundamental frequencies of the Mean 3 and RMS block on settling time delay after three phase fault 35

Figure 22 Effect of changing the load Q_f on islanding detection waveform output 36

Figure 23 Variations in the ROCOF waveform during (a) Islanding event with zero power mismatch and (b) Three phase short circuit fault (non-islanding event) 37
Figure 24 Block diagram of proposed detection technique 37
Figure 25 Waveforms of voltage amplitude for different event types 38
Figure 26 Waveforms of voltage amplitude for similar event types 39
Figure 27 Structure of a feedforward neural network 39
Figure 28 A layer of neurons in an Artificial Neural Network 40
Figure 29 Proposed approach for DG event classification 42
Figure 30 Simulink models of (a) DG System. (b) Utility grid 44
Figure 31 Results for zero mismatch scenario. (a) Islanding detection waveform. (b) Islanding detection signal 46
Figure 32 Results for real power mismatch scenarios. (a) Islanding detection waveform. (b) Islanding trigger signal 47
Figure 33 Results for reactive power mismatch scenarios. (a) Islanding detection waveform. (b) Islanding trigger signal 48
Figure 34 Results for fault and loss of parallel feeder. (a) Islanding detection waveform. (b) Islanding trigger signal 48
Figure 35 Results for load and capacitor bank switching (a) Islanding detection waveform. (b) Islanding detection signal 49
Figure 36 Setup to test the effect of starting an industrial motor 50
Figure 37 Effect of 100 kVA motor starting on (a) RMS Voltage waveform at PCC (b) Islanding detection waveform 50
Figure 38 Model containing two DGs in parallel 51
Figure 39 Taxonomy of islanding and non-Islanding Simulated Events 52
Figure 40 IDW and $O_{detection}$ for a) Zero mismatch b) 25% real power deficit c) 1% reactive power deficit 53
Figure 41 IDW for islanding with zero mismatch for different DG capacities 54
Figure 42 IDW and $O_{detection}$ for different switching events 55
Figure 43 IDW and $O_{detection}$ for (a) Three phase fault (b) Loss of parallel feeder (c) Motor starting 55
Figure 44 Change of misclassification rate for two different ANNs 57
Figure 45 Confusion matrix for the optimized ANN trained with V_{pu} values 57
Figure 46 Confusion matrix for the optimized ANN trained with frequency values 58
Figure 47 DG event classification technique block diagram 60

List of Tables

Table 1 Islanding detection requirements set by interconnection standards 7
Table 2 Comparison of existing islanding detection techniques 24
Table 3 Comparison of existing event classification techniques 28
Table 4 Parameters selected for event classification 41
Table 5 Organization of input matrix to neural networks 41
Table 6 Details regarding ANN transfer function and training algorithm selection . . . 42
Table 7 Specifications of the simulation model 45
Table 8 Islanding and non-islanding scenarios simulated 46
Table 9 Maximum time delays for various non-islanding events 49
Table 10 Effect of change of DG nominal power 51
Table 11 Comparison between values obtained from single and double DG simulations . 52
Table 12 Simulated cases for DG event classification 56
Table 13 Optimized classification performance of various ANNs 56
Table 14 Event number and description in the confusion matrices 59
Table 15 Classification accuracy in the majority vote for different combinations of ANNs 59
Table 16 Classification accuracy for each event 59

Chapter 1

INTRODUCTION

The conventional electric power grid model consists of centralized power plants supplying bulk quantities of power to consumers through long distance transmission lines. The centralized nature of the grid has made it extremely vulnerable to contingencies such as severe weather, transmission line or plant outages which result in cascading failures and widespread blackouts (Hines, Apt, and Talukdar 2009). Furthermore, the increase in the world's energy demand has strained the grid to its limits (DOE 2013). This is because of economical and environmental constraints restricting new power plant construction and prohibitive costs in transmission infrastructure upgrades. The distributed power generation model is thus being widely advocated as an alternative because it complements the centralized model by meeting local demand, avoiding the long distance transmission power losses, and reducing the cost of upgrading the transmission system infrastructure (Heeter and Nicholas 2013; REN21 2014; Bayod-Rújula 2009). This model consists of distributed generation (DG) units, which are decentralized electrical power sources connected to the grid at the distribution level (Ackermann, Andersson, and Söder 2001). DG sources are typically classified as synchronous or inverter-based systems. For instance, small gas-fired machines used as backup units are classified as synchronous generators while renewable energy sources such as wind and solar are inverter-based units. The distributed model consists of small DG units spread over a wide area. Therefore, the model is more reliable since the failure of a small unit can be easily compensated for by the rest of the units. A considerable fraction of DG sources are renewables sources such as photo-voltaic arrays, wind energy conversion systems, fuel cells, mini hydro power plants, etc (Bayod-Rújula 2009). These renewable sources have the added benefit of being environmentally friendly and thus help meet environmental and sustainability targets such as the European Union's 20/20/20 vision. Renewable energy based DG systems also enhance the energy security of a region, since the source of energy is locally available.

In spite of numerous benefits, there are still several challenges imposed due to the integration of DG into the power distribution systems (Bayod-Rújula 2009). These challenges lead to the degradation of operational stability of the entire grid and also present serious safety hazards to electrical equipments and lives. The solution to such challenges lies in the research regarding the evolution of the current power grid into a smart grid. An important aspect of such research efforts is to decentralize the operational intelligence and control of the system. Therefore, DG systems of the

future will eventually be incorporated with adequate intelligence to autonomously tackle challenges related to local operational stability and protection, i.e., such DG systems will become smart. Two different aspects of smart DG systems; improved islanding detection and event classification; are addressed in the following sections.

Islanding Detection

Islanding is a major challenge to the integration of DG units into the power system. Islanding occurs when the system containing the DG is electrically disconnected from the rest of the power grid. This can happen due to many reasons including faults, substation failure or equipment malfunction (Walling and Miller 2002). Figure 1 shows a scenario of a DG system being islanded due to a fault on the line connecting the DG to the grid.

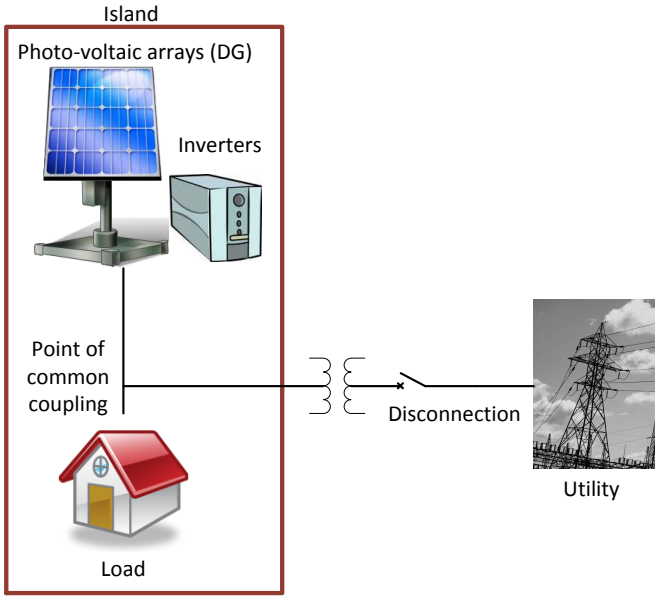

Figure 1. A typical islanding scenario

Prolonged islanding leads to a variety of safety hazards (Laghari et al. 2014). If the DG protection system does not detect islanding and take appropriate measures, then power is being unintentionally fed back by these DG sources. For instance, power lines disconnected from the grid can still be energized by a nearby DG source presenting serious safety hazards to field engineers and maintenance personnel. Moreover, most of the existing DG systems are independently owned and electric utilities have limited or no control over such DG units. When islanding occurs, the DG voltage in that isolated area will lose phase synchronization with the rest of the power system. Reclosing in such a condition could introduce damaging high currents and torques into the power grid. Automatic reclosing after faults may even fail to function if the DG source keeps on feeding

the fault in islanding mode. In this case, manual reclosing would be required to clear the fault resulting in unnecessarily prolonged grid disconnected period. Therefore, international and national standards dealing with the interconnection of distributed generation sources to the power grid such as the IEEE 1547 series (IEEE1547 2009), IEC 62116 (IEC62116 2009), and UL1741 (UL1741 2001) mandate that every DG system must have its own islanding protection capability. If the DG is able to maintain voltage and frequency in the island, then it will be allowed to operate autonomously, otherwise it would be required to shut down.

There have been considerable efforts to develop an accurate, fast and robust islanding detection technique (IDT) to facilitate increased penetration of DG sources into the grid. They can be broadly classified into passive, active, machine learning and remote detection techniques as shown in Figure 2.

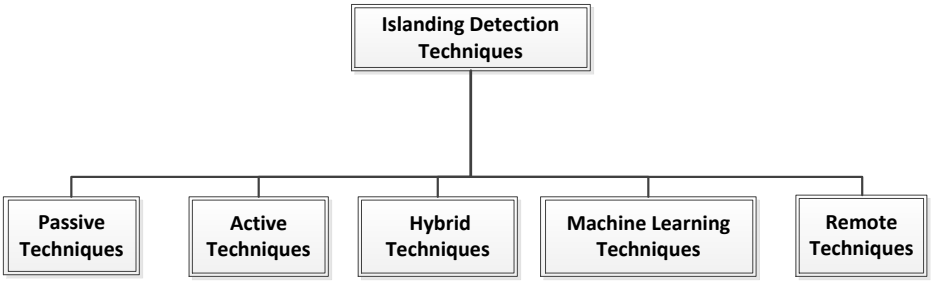

Figure 2. Taxonomy of islanding detection techniques

Passive techniques generally monitor one or more parameter at the point of common coupling (PCC) between the DG system and the grid to detect islanding when these parameters change beyond the predefined thresholds. Active techniques destabilize the island by continuously varying the amplitude, phase or frequency of the DG output current waveform. Hybrid techniques augment the performance of passive techniques by enabling active techniques only under certain operating conditions. Machine learning detection techniques are based on machine learning algorithm that can be trained to detect islanding using large sets of sample data representing islanding and non-islanding events. Remote techniques are based on either sensing signals transmitted from the utility side or measuring the relative difference between remote and local power system parameters to detect islanding. Out of the various types of IDTs, passive techniques are the most widely implemented because they are generally computationally inexpensive and can be easily integrated into the DG system. However, they cannot detect islanding under certain operating conditions and may falsely detect islanding during other power system disturbances. Therefore, two novel passive IDTs which eliminate non-detection and false triggering issues of passive techniques were proposed. These tech-

niques are designed for inverter-based DG systems because they represent the largest and the fastest growing DG sector (REN21 2014). In grid-connected mode, the the rate of change of frequency and voltage amplitude waveforms remain steady due to the stabilizing effect of the grid. After islanding occurs, these waveforms show sustained ripples because of the imperfections in the DG control system. Therefore, the proposed techniques are based on monitoring the ripple content in these waveforms. Islanding is detected when the ripple content in the monitored waveform exceeds a predefined threshold for a specific amount of time. The monitoring is performed in the time domain which simplifies their integration in DG inverters. The proposed techniques have been tested with a wide range of islanding and non-islanding scenarios to validate their islanding detection capability. Both of the techniques were able to successfully detect islanding under all tested conditions and were also able to successfully distinguish between islanding and non-islanding events.

Event Classification

Utility operators have to maintain constant voltage and frequency throughout the power grid to ensure normal operation of the system (Mahela, Shaik, and Gupta 2015). They have extensive monitoring and data acquisition capability to capture event data during power system disturbances. This data is then processed to extract features from local parameters to be used for identifying and classifying various disrupting events. Such classification helps to develop a clear understanding of the operating requirements needed to mitigate the impact of such events on the power system. However, due to the centralized nature of the power grid, only the central utility operators have access to the data and only they get to make the operating decisions. Current research in smart grid aims to make the monitoring and control of the power grid much more decentralized, so that each subsystem has its own monitoring and control capability. There has been extensive research efforts by utilities and power research institutes to develop advanced event classification techniques which are highly accurate and robust (Saini and Kapoor 2012). The proposed techniques rely on spectral transform techniques to extract features to be used by machine learning based classifiers. More details about these techniques are provided in Section 2. However, most of the research focus on large and complicated power systems consisting of large centralized generators and loads. There is very little research which focus exclusively on the classification of events local to DG systems. If DG systems are augmented with event classification capability, the DG operators can monitor the impact of such events and devise algorithms to mitigate any negative effects of such events in the future. For example, the DG might want to intentionally island during severe faults or loss of parallel feeder scenarios because of the possibility of cascading failures in the aftermath of such

events. Since event data varies from point to point, local classification by DG systems would be much more accurate compared to classification based on data representing a large and complicated power system. The classification results can also be communicated to the utility, which can be utilized in wide area monitoring and control. Comparative analysis of the results from DGs in a wide area can help utility operators determine the location of an event like a short circuit fault or a loss of parallel feeder.

The proposed DG event classification technique is a novel research effort towards a smart DG system. The technique monitors and logs a certain combination of local parameters which are used as inputs to a set of artificial neural networks (ANN) trained to classify the local event. Each ANN is trained to classify based on values obtained from a single parameter only. The classification output of all the ANNs are analyzed and the majority vote is selected as the final classification output. The model of the technique has been optimized to reduce the computational burden while maintaining classification accuracy. The performance of the technique has been validated using ten-fold cross-validation of a large dataset of local events. The technique can successfully classify critical events such as islanding, different type of short circuit faults, loss of parallel feeder, load switching and capacitor switching with an accuracy of over 98%. Furthermore, it is also able to characterize the island based on the type of power mismatch (real or reactive), which can help the system operator decide on the operating action needed after islanding. The rest of this thesis is organized as follows:

In chapter 2, a review on the existing islanding detection and event classification techniques has been provided. In chapter 3, the technical details of the proposed islanding detection and event classification techniques have been discussed. Chapter 4 discussed the simulation model used to test the proposed techniques and then presents the results of the different techniques alongwith a detailed performance analysis. Finally, in chapter 5, a review of the contribution of this work has been presented alongwith a summary of the key findings and future research direction.

Chapter 2

LITERATURE REVIEW

There has been extensive research regarding improved islanding detection and power system event classification in recent years. This chapter presents a detailed review of the existing islanding detection and event classification schemes.

Islanding Detection Standards and Non-Detection Zones

The increased DG penetration into the power grid in recent years has given rise to several international standards which provide guidelines on interconnection of DG into the power grid. Some of the important standards are:

- IEEE 1547 series of standards for interconnection of distributed resources with electric power systems (IEEE1547 2009)
- UL 1741 standard for safety for static converters and charge controllers for use in photovoltaic power systems (UL1741 2001)
- IEC 62116 standard test procedure for utility-interconnected photovoltaic inverters (IEC62116 2009)

Each of these standards has a sizable portion devoted to islanding detection requirements. The main requirements set by these standards are the maximum detection time, the voltage and frequency thresholds and the maximum load quality factor. Table 1 lists the values of these parameters for the different standards. A maximum time of 2 seconds is allowed by all the standards to detect islanding. Moreover, the DG protection device such as inverter or relay needs to shut down the system when the system voltage or frequency goes beyond the given thresholds. The load quality factor (Q_f) is defined as the ratio of the load reactive power to the rated real power provided by the DG source. Generally, islanding detection techniques use frequency, voltage and power parameters for detection. A change in load Q_f affects each of these parameters, which in turn affects the performance of the technique.

Islanding detection technique (IDT) performance is benchmarked using its detection time, accuracy in distinguishing islanding events from non-islanding events and non-detection zone(NDZ). Before discussing the various IDTs, a brief introduction of Non-Detection Zones (NDZ) is presented.

Table 1. Islanding detection requirements set by interconnection standards

Standard	**Detection Time (s)**	**Frequency Range (Hz)**	**Voltage Range**	**Load Q_f**
IEEE 1547	2	59.3< f <60.5	88%< V <110%	1
UL 1741	2	59.3< f <60.5	88 % < V < 110 %	2.5
IEC 62116	2	58.5 < f < 61.5	85 % < V < 115 %	1

NDZ is generally defined as the operating range of active (ΔP) and reactive power (ΔQ) mismatch where islanding is not detected by the technique. Figure 3 (a) shows a general representation of NDZ for passive and active techniques.

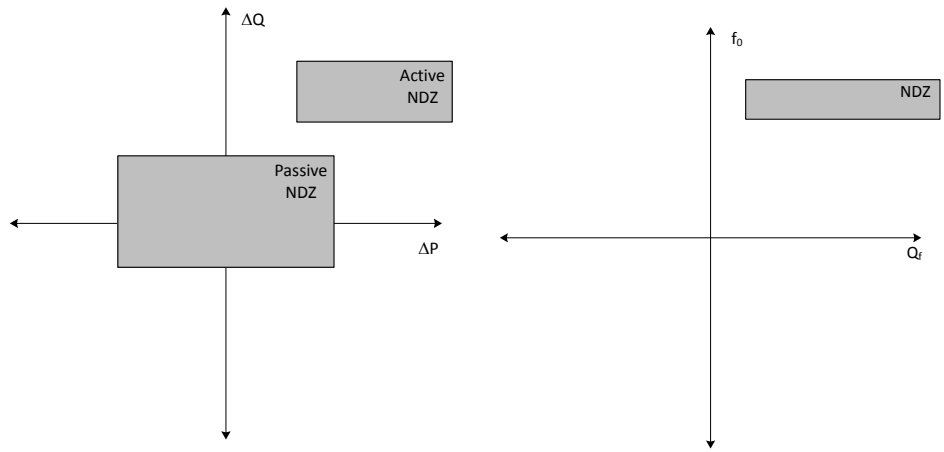

(a) (b)

Figure 3. NDZ representation of (a) passive and active techniques in active/reactive power mismatch domain (b) active techniques in frequency-Q_f domain

Passive techniques have NDZ for small power mismatches because the monitored parameter generally stays within the thresholds. Active techniques have NDZs under conditions when the injected disturbance actually compensates for the power mismatch in the island. These techniques rely on destabilizing the island and thereby triggering protection devices to shut the island down. Loads with high Q_f at resonant frequency (f_0) tend to neutralize the destabilizing impact of such techniques and can lead to failure in island detection. Therefore, the NDZ of active techniques can also be represented in f_0-Q_f domain as shown in Figure 3 (b). Hybrid techniques have smaller NDZs than active or passive techniques. Machine learning techniques are evaluated according to their classification accuracy and therefore they have no distinct NDZ in these domains. Remote techniques do not exhibit NDZ because they only rely on two-way communication between the DG and utility.

Passive Islanding Detection Techniques

Passive techniques monitor the change in system parameters such as voltage, frequency, and current in the DG side at the point of common coupling (PCC). In case of islanding, these parameters exhibit considerable variations. Figure 4 presents some of the common passive IDTs which are discussed throughout the remainder of this section.

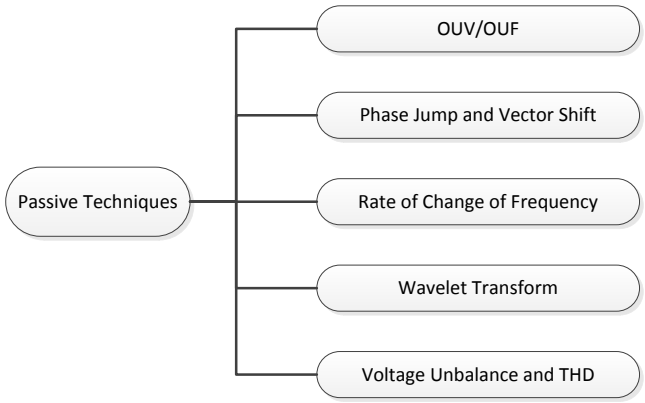

Figure 4. Types of popular passive techniques

Over-Under Voltage and Frequency

Over-under voltage and over-under frequency (OUV/OUF) protection is required by interconnection standards to be installed in all modern DG protection systems (Bower and Ropp 2002; Khamis et al. 2013). Besides islanding detection, they also serve to protect the system against any abnormal voltage and frequency excursions during grid-connected mode. In these techniques, the voltage and frequency are constantly monitored at the PCC. If the observed parameter deviates from a preset threshold value (Table 1), the DG source is turned off. Figure 5 shows the single line diagram of a grid-connected DG source. The real power (ΔP) and reactive power (ΔQ) delivered are represented by Equations 2.1 and 2.2 respectively. P_{DG} and Q_{DG} are the real and reactive power delivered by the DG source respectively. Similarly, P_{load} and Q_{load} are the real and reactive power absorbed by the load.

$$\Delta P = P_{DG} - P_{load} \tag{2.1}$$

$$\Delta Q = Q_{DG} - Q_{load} \tag{2.2}$$

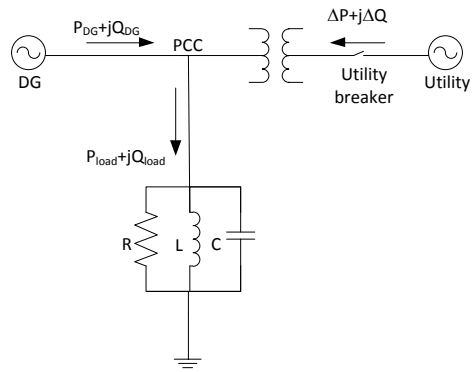

Figure 5. A typical system model of a grid-connected DG source

If $\Delta P \neq 0$, the PCC voltage (V_{PCC}) will fluctuate from the nominal levels indicating islanding conditions. Similarly, if $\Delta Q \neq 0$, the system frequency will change if islanding occurs. When the power demand is not met, the voltage and frequency will exceed the threshold levels and quickly trigger islanding detection. However, these detection techniques have large NDZ which are determined by the equations,

$$\left(\frac{V}{V_{max}}\right)^2 - 1 \leq \frac{\Delta P}{P} \leq \left(\frac{V}{V_{min}}\right)^2 - 1 \tag{2.3}$$

$$1 - \left(\frac{f}{f_{min}}\right)^2 \leq \frac{\Delta Q}{P} \leq 1 - \left(\frac{f}{f_{max}}\right)^2 \tag{2.4}$$

According to IEEE 1547 series, $V_{min} = 0.88pu$, $V_{max} = 1.1pu$, $f_{min} = 59.3Hz$, and $f_{max} = 60.5Hz$. Therefore, the corresponding NDZ in real and reactive mismatch are:

$$-17.36\% \leq \frac{\Delta P}{P} \leq 29.13\% \tag{2.5}$$

$$-5.94\% \leq \frac{\Delta Q}{P} \leq 4.11\% \tag{2.6}$$

The probability of the load being in the NDZ can be as high as 30% at certain times of day under large DG penetration (Stevens et al. 2000). Furthermore, other non-islanding scenarios such as short circuit faults, capacitor and load switching events, etc can falsely trigger these schemes since they also affect system voltage and frequency.

Phase Jump and Vector Shift Detection

The phase jump technique monitors the phase difference between the inverter's terminal voltage and the output current (Bower and Ropp 2002). Most of the inverter-based DG are designed to operate in unity power factor mode. After islanding, due to the reactive nature of the load, a phase jump will occur, as shown in Figure 6. Therefore, islanding can be detected when the phase difference suddenly goes beyond some threshold. This technique is very easy to implement in inverters since PLLs are already used in inverters to monitor phase difference for utility synchronization. However, the threshold selection for this technique is difficult because events like motor starting and faults can also cause similar phase shifts. In addition, this technique will not be able to detect islanding for loads with very small phase angles at utility frequency.

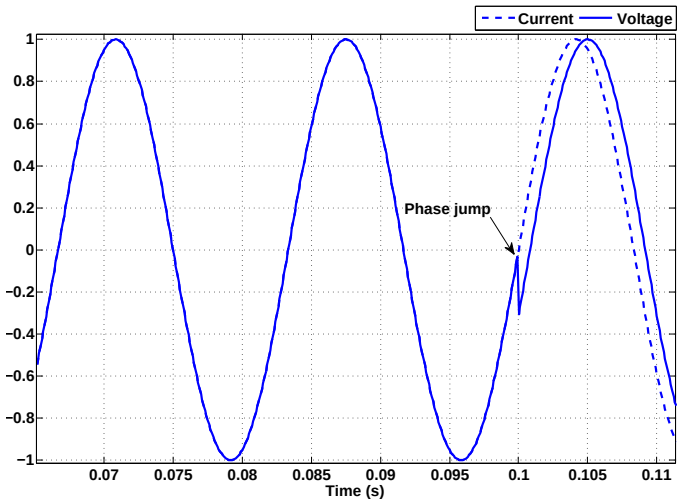

Figure 6. Phase shift during islanding

Vector shift is a similar technique which is implemented in relays designed to protect synchronous generators. The load angle, i.e. the angle difference between the terminal voltage and the generator electromagnetic force (EMF), is monitored for a sudden change to detect islanding (Freitas and Xu 2004). In a grid-connected DG system, the load current is generally shared by the DG and the utility. After islanding, however, the DG has to supply all the needed current to the load. This change in the load to be supplied by the DG leads to a sudden voltage drop across the generator impedance which in turn causes the load phase to shift. This technique also cannot detect islanding if the power mismatch is small after islanding and is prone to nuisance tripping during short circuit faults and motor startups.

Rate of Change of Frequency-based Techniques

The rate of change of frequency (ROCOF) has been used to detect islanding for synchronous generator-based DG systems because it is related to the difference in the DG power output (P_{DG}) and the load demand (P_{load}), as represented by the following equation,

$$\frac{df}{dt} = \frac{P_{DG} - P_{load}}{2 \cdot H \cdot G} \tag{2.7}$$

where f is the DG frequency, H is the generator inertia constant and G is the rated generation capacity. However, it still has a large NDZ because the ROCOF is directly proportional to the power mismatch. Rate of change of frequency over power is another detection index used for islanding detection (Pai and Huang 2001). Its NDZ is significantly reduced but it still cannot detect islanding if the power mismatch is very small.

Wavelet Transform

Wavelet transform is a signal processing technique used to estimate the frequency components for non-stationary signals, i.e., signals whose frequency components vary with time (Ruqiang and Gao 2009). It does this by partitioning the signal into variable time windows, the size of which depends on the frequency component to be analyzed. A template function called the base or mother wavelet is chosen from the signal which is then time-scaled (dilated or contracted), time-shifted (translated along time axis) and compared with signal for similarities. These transforms have been applied to extract useful information from current and voltage signals and to calculate suitable parameters for islanding detection.

Khamis et al. have provided a detailed review of the different types of wavelet-transform based techniques used to detect islanding (Khamis et al. 2013). Although these detection techniques can be very accurate, they are computationally expensive and not trivial to incorporate within existing protection equipment.

Total Harmonic Distortion and Voltage Unbalance-based Techniques

Harmonics are generated in the voltage and current signals due to the switching operation of the PV inverter. Figure 7 illustrates the difference in harmonic current flow between grid-connected and islanded conditions.

The harmonics flow into the low impendance grid under normal conditions. In the absence of the grid, the harmonic currents flow into the islanded load and increase the V_{PCC} harmonic

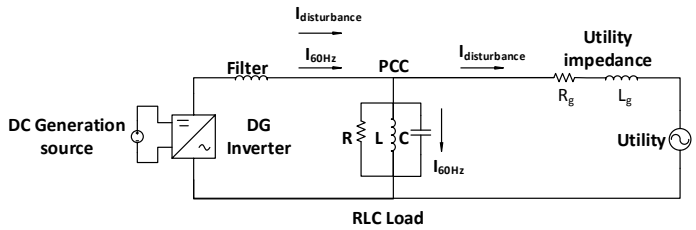

(a) Grid-connected condition

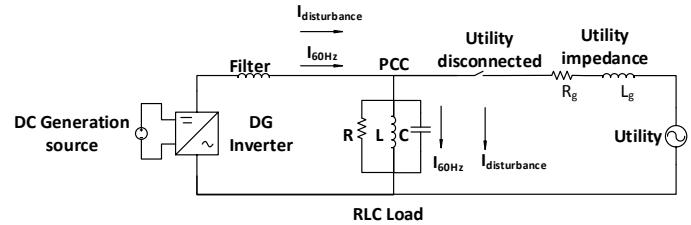

(b) Islanded condition

Figure 7. Harmonic current flow in an inverter based system for (a) grid-connected and (b) islanded conditions

level (Bower and Ropp 2002). Therefore, Total Harmonic Distortion (THD) of V_{PCC} or the inverter output current (I_{inv}) can be used to detect islanding.

However, the threshold selection in such techniques is very difficult since non-linear loads can increase the harmonic level in the grid-connected systems and lead to false detection. This inherent limitation in the THD-based detection techniques has led to the use of Voltage Unbalance parameter (Jang and Kim 2004; Laaksonen 2013). Voltage unbalance is the ratio between the negative and positive voltage sequences. If NS_t and PS_t represent the magnitude of the negative and positive voltage sequence at time t, then, voltage unbalance at t (VU_t) can be mathematically represented as:

$$VU_t = \frac{NS_t}{PS_t} \times 100 \tag{2.8}$$

The change in the topology of the power system results in an abrupt change in VU_t, even for small power mismatch conditions. Therefore, the VU_t values are used alongwith THD to improve the detection accuracy. This technique has been augmented with a logic decision block which determines whether the island is sustainable or not (Laaksonen 2013). The island will be allowed to operate if its generation source is capable of sustaining the load. However, this technique is computationally expensive and its threshold selection is system dependent. Furthermore, this technique will not work for single phase systems, since VU_t is based on three phase voltage measurements.

Active Islanding Detection Techniques

Active techniques inject distortions in the inverter output current waveform by changing its amplitude, phase or frequency. In a grid-connected condition, the distortions get absorbed by the grid. However, when the DG is islanded, these distortions are designed to drive the operating point of the island to a level that triggers the system protection devices. Figure 8 presents a broad classification of the different active techniques discussed.

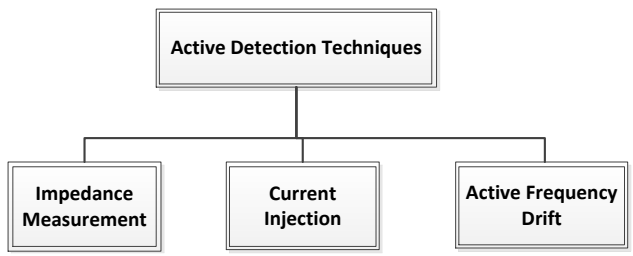

Figure 8. Taxonomy of active detection techniques

Impedance Measurement Techniques

These techniques add new frequency components into the inverter output current (I_{inv}) and measure the voltage at the corresponding frequency to determine the impedance (Asiminoaei et al. 2005; Tedde and Smedley 2014; Cai et al. 2013). The equivalent impedance (Z_{Equi}) in a grid-connected system is usually smaller than in an islanded system due to the presence of the low-impedance (Z_{Grid}) grid connected in parallel with the load (Z_{Load}). This is illustrated in Figure 9 and Equation 2.9.

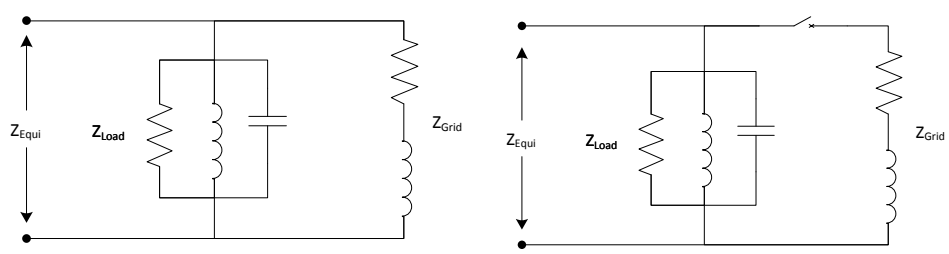

(a) Grid-connected condition (b) Islanded condition

Figure 9. Equivalent impedance seen by the DG during (a) grid-connected and (b) islanded conditions

$$Z_{Equi} = \begin{cases} Z_{Load}||Z_{Grid} & if \;\; grid\, connected \\ Z_{Load} & if \;\; islanded \end{cases} \tag{2.9}$$

The selection of the harmonic frequency is critical since the grid voltage waveform contains characteristic harmonics (third, fifth and seventh order) which can interfere with the impedance measurement. Injection of distortions having frequency components lying in between successive or-

ders of harmonics have been proposed (Asiminoaei et al. 2005; Cai et al. 2013) since they are not typically present in the grid. Tedde et al. also proposed the injection of distortions having frequency lower than that of the fundamental component since these are not present in the grid either (Tedde and Smedley 2014). Du et al. (Asiminoaei et al. 2005) proposed the use of harmonic compensators to eliminate the characteristic harmonics and thereby aiding in the impedance measurement. Cai et al. (Cai et al. 2013) proposed injection of dual-frequency interharmonic components to improve the performance of the single harmonic injection technique. However, the injection of such harmonic currents adds to the harmonic content of the grid. Therefore, the amplitude of the harmonic components has to be very small so that the THD of the output remains under $< 5\%$ as required by the interconnection standards (IEEE1547 2009).

Current Injection Techniques

These techniques inject currents in the dq-frame (Hernandez-Gonzalez and Iravani 2006; Gupta, Bhatia, and Jain 2015). The dq transform (also called the park's transform) is a space vector transformation which converts the 3-phase signals from a stationary (ABC) frame to a synchronously rotating (dq) frame. In the dq frame, the 3-phase signals are divided into orthogonal components (Crowhurst et al. 2010). The main advantage of this transformation is that the inverter active and reactive power output can be independently controlled by the dq components. The relationships between the real(p) and reactive(q) output power and the dq components are:

$$p = \frac{3}{2} v_d i_d \tag{2.10}$$

$$q = \frac{3}{2} v_d i_q \tag{2.11}$$

where i_d is the d-axis current, i_q is the q-axis current and v_d is the d-axis PCC single-phase voltage.

Gonzalez and Iravani investigated the effect of injecting both i_d and i_q currents at a certain frequency(ω_d) (Hernandez-Gonzalez and Iravani 2006). In grid-connected conditions, such injections have no effect. However, in an islanded condition, i_d injection results in voltage v_d having an additional ω_d component while i_q injection causes the system frequency to deviate. The islanded system frequency deviates because it is dependent on the reactive power mismatch in the system, which is being controlled by the amount of i_q injection. The amplitude of ω_d is very small due to i_d injection and is dependent on the system parameters. Therefore, they proposed islanding detection

by i_q injection and monitoring the associated frequency deviation. However, this method failed to detect islanding for loads with $Q_f > 3$. Gupta et al. added to this work by proposing an index called Average Absolute Frequency Deviation Value ($AFDV_{AG}$) (Gupta, Bhatia, and Jain 2015). As the name suggests, this index is representative of the average frequency deviation in the system. Thresholds have been chosen such that the technique detects for zero mismatch conditions with high Q_f loads. Two different thresholds, namely $Threshold1$ and $Threshold2$, have been selected for i_q injection components of frequency 30 Hz and 20 Hz respectively. These thresholds have been chosen such that the technique detects for zero mismatch conditions with high Q_f loads. Initially, the frequency of i_q injection is 30 Hz. If the $AFDV_{AG} > Threshold1$, islanding is suspected and the frequency of i_q injection is changed to 20 Hz. If $AFDV_{AG} > Threshold2$, then islanding is detected. This reconfirmation of islanding, once it is suspected, is done to avoid the possibility of nuisance tripping due to non-islanding events.

Active Frequency Drift Techniques

These techniques reinforce the frequency deviation resulting due to islanding to drive the system frequency beyond the thresholds set by protection devices installed in the DG. The conventional active frequency drift (AFD) technique slightly increases the frequency of the inverter output current (I_{inv}) every half cycle, compared to the undistorted sinusoidal waveform (Ropp, Begovic, and Rohatgi 1999). That is, it stays at zero for a time t_z until the beginning of the second half-cycle of the original sinusoid. A ratio called the chopping fraction has been introduced to quantify the effect of t_z. Chopping fraction (cf) is defined as the ratio of t_z to half time period of the voltage waveform (T_{grid}) i.e.,

$$cf = \frac{2t_z}{T_{grid}} \tag{2.12}$$

Figure 10 shows the V_{PCC} before islanding and I_{inv} of an inverter employing AFD. After islanding, V_{PCC} follows the sinusoidal component of I_{inv}. This causes the rising zero crossing of V_{PCC} to occur sooner than expected and leads to a phase error between V_{PCC} and I_{inv}. The inverter detects this phase error and increases its output frequency to synchronize the zero crossings of the current waveform with that of the voltage, so that the system power factor remains at unity. However, due to the presence of the distortion in I_{inv}, V_{PCC} still has a phase error and the inverter keeps changing its frequency to synchronize the two waveforms. This process repeats itself till the system frequency deviates so much that the protection devices get triggered and shut down the

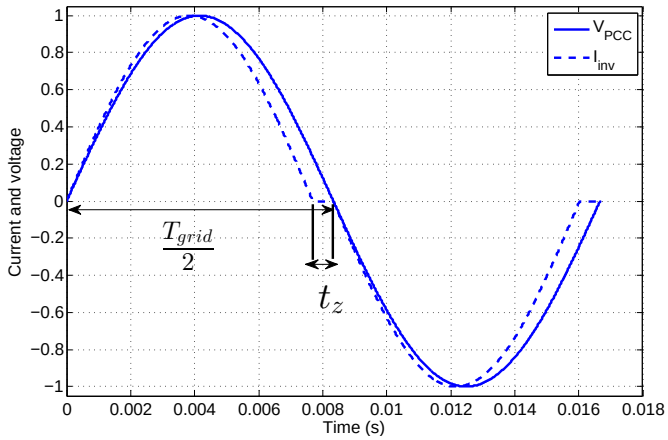

Figure 10. PCC voltage and output current waveform of an inverter applying active frequency drift

islanded system. However, this method fails for high Q_f loads unless t_z is made considerably large. However, a high value of t_z is generally not employed because it introduces unacceptably high values of THD during normal operation.

To enhance the performance of the conventional AFD technique, Sandia National Laboratories proposed the changing of the chopping fraction of I_{inv} according to the instantaneous frequency deviation ($\Delta\omega$). The relation is given in Equation 2.13 (Stevens et al. 2000).

$$cf_k = cf_{k-1} + F(\Delta\omega_{k-1}) \tag{2.13}$$

where cf_{k-1} and $Delta\omega_{k-1}$ are the chopping fraction and the frequency deviation in the previous cycle respectively.

This technique is called the Sandia Frequency Shift (SFS) method. In an islanded condition, the frequency change results in a deviation in cf which eventually causes the PV inverter to change its frequency. Therefore, this technique utilizes frequency deviation as positive feedback to drive the system frequency to the OUF threshold level. Similarly, Sandia Voltage Shift (SVS) is another method that uses V_{PCC} amplitude as positive feedback to detect islanding. In this technique, I_{inv} is changed whenever there is a change in V_{PCC} amplitude. During islanding, this change in I_{inv} causes the inverter output power to change which in turn introduces further deviation in V_{PCC}. This process continues until V_{PCC} reaches OUV threshold. SFS has been simultaneously tested with the SVS method showing very low NDZ (Bower and Ropp 2002).

Slip Mode Frequency Shift (SMS) is another technique which utilizes positive feedback in frequency deviation to detect islanding (Khamis et al. 2013). In this technique, I_{inv} is programmed

as,

$$I_{inv} = \sqrt{2}I[2\pi f_{k-1}t + \theta_{SMS}] \tag{2.14}$$

$$\theta_{SMS} = \theta_m sin(\frac{\pi f - f_g}{2f_m - f_g}) \tag{2.15}$$

where θ_m is the maximum phase angle at frequency f_m, f_g is the nominal system frequency and f is the measured frequency. The value of θ_{SMS} is designed to increase with the deviation of the system frequency from the nominal frequency. In an islanded system, slight deviations in f will lead to high values in θ_{SMS} and this provides positive feedback to the frequency deviation itself. This process goes on till the system operating crosses the OUF limits.

Estebanez et al. (Estebanez et al. 2011) investigated the comparative performance of AFD, SMS and SFS techniques. They concluded that for islanding detection, SMS techniques exhibit the best performance in terms of NDZ and THD content under normal operating conditions.

Hybrid Islanding Detection Techniques

These techniques augment the performance of passive techniques with active techniques. The active component of the technique is employed only when the passive component fails to detect islanding, i.e., disturbances are introduced into the system only when the monitored parameter exhibits certain abnormal spikes which are within islanding detection thresholds.

Akhlaghi et al. (Akhlaghi, Ghadimi, and Akhlaghi 2014) proposed a hybrid technique which uses a combination of SMS and reactive power–frequency ($Q - f$) droop alongwith the passive OUV/OUF technique. Both of the active techniques are designed to change the frequency of an island. The SMS technique changes the phase angle of the inverter output current whenever the system frequency deviates from the nominal frequency, and this has the effect of positive feedback on the frequency deviation during an islanding condition. The $Q - f$ droop technique changes the reactive power setting of the DG. In an islanded condition, this has the effect of changing the system operating frequency. However, each of these techniques have certain issues when employed independently. The SMS technique performs poorly for constant power controlled inverter, which try to keep the frequency constant. The $Q - f$ droop technique takes a long time to detect and is also not able to detect for loads with high quality factor. But when these two techniques are employed simultaneously, islanding is detected quickly, even for loads with high quality factor.

Menon and Nehrir (Menon and Nehrir 2007) proposed a technique which changes the frequency setting of the DG if a spike in the Voltage Unbalance (VU_t) value is detected. VU_t is the

ratio between the negative and positive voltage sequences. Spikes in VU_t can occur during changes in power system topology. In grid-connected scenarios, the change in the DG frequency setting has no effect on the system frequency because the grid is designed to maintain a constant frequency. However, after islanding, this has the effect of deviating system frequency beyond the protection thresholds and leading to islanding detection.

Mahat et al. (Mahat, Chen, and Bak-Jensen 2008) proposed a technique which shifts the real power reference setting when the average rate of voltage deivation shows small but steady deviations. This has the effect of increasing the rate of voltage change significantly during islanding and this characteristic is used to detect islanding.

Chang (Chang 2010) proposed a technique which used Rate of Change of Frequency (ROCOF) and rate of change of voltage (ROCOV) as passive techniques and an active technique which switches in and out a high impedance load and measures the corresponding PCC voltage variation. The active technique is only employed when small but sustained ROCOF and ROCOV values are observed. A correlation factor (CF) between the PCC voltage and the source of voltage perturbation is used to classify between islanding and non-islanding. In islanding conditions, CF would be high since PCC voltage would fluctuate more with load switching. Laghari et al. (Laghari et al. 2013) proposed a similar technique in which changes in the rate of change of reactive power (ROCORP) are monitored and extra loads are connected if small reactive power variations are detected. This has the effect of amplifying the ROCORP values in islanded conditions.

Machine Learning-based Detection Techniques

Machine learning techniques use adaptive algorithms that can be trained to classify the islanding and non-islanding events. These algorithms learn from sample input and output data, then construct models which can make classification decisions based on their inputs. Islanding detection has been proposed by using algorithms with a large dataset of input parameters alongwith the taget class (islanding or non-islanding). Figure 11 presents the different machine learning techniques reviewed in this paper.

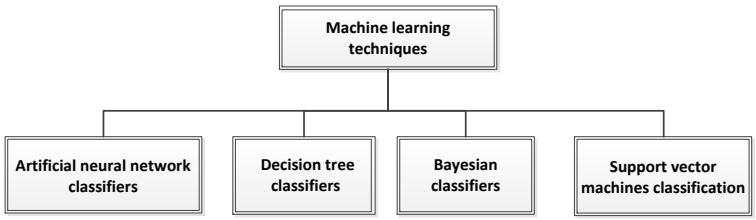

Figure 11. Common types of machine learning based detection techniques

Artificial Neural Networks

Artificial Neural Networks (ANN) are popular mathematical models which can be applied for various applications like pattern recognition, function fitting, signal forecasting, etc. They belong to a type of machine learning algorithm whose logic is inspired by the model of the biological brain. In the domain of power systems, these features have been utilized in fault classification, voltage stability analysis, design of power system stabilizers, etc (Aggarwal and Song 1998). The basic structure of an ANN is a highly interconnected network consisting of an input layer, one or more hidden layers and an output layer. The hidden layers are called neurons and the designer has to choose how many neurons to use for his/her application. Higher number of neurons generally result in better performance but require more time to train the network and increase the complexity of the system.

There has been extensive research in recent years regarding the application of ANN and its islanding detection capabilities. Salman et al. presented the application of ANN for islanding detection by using three phase voltage and current signals as input to the network (Salman, King, and Weller 2004). The algorithm was designed to train itself to distinguish islanding from grid-connected disturbances. A software tool called PREDICT was used to design an optimal network, which simplifies the network as much as possible and use the least number of parameters for that purpose. This was achieved by starting with the simplest network consisting of input layers being directly connected to output layers. Then, it kept on adding neurons until an optimum performance was established. Results showed that the optimum network contained 10 neurons and had a classification rate of 98-99%. Fayyad et al. proposed an ANN based IDT for multiple DGs using transients in voltage signals (Fayyad and Osman 2010). Wavelet transform was used to extract spectral co-efficients from the transients and then these co-efficients were used to train the ANN to distinguish between islanding and non-islanding events. A total of 360 islanding and non-islanding cases were generated to test the performance of the system. The technique was evaluated using 3-fold cross-validation and exhibited an overall accuracy of 97%. Ahmad et al. proposed an ANN-based IDT for DFIG wind turbines using symmetrical components of the second harmonic frequency of the voltage and current signals (Abd-Elkader, Allam, and Tageldin 2014). Fourier transform was used to obtain the second order harmonics. The ANN was a two-layered feedforward network with sigmoid hidden and output neurons. This technique was reported to be fast in distinguishing between islanding and non-islanding events. However, no details of overall classification accuracy was presented.In addition, this technique failed to detect islanding when there is a significant power mismatch in the island. Moeini at al. presented an ANN-based IDT for synchronous DGs which trained the network using the input signals of the automatic load frequency controller of the DG (Moeini et al. 2011).

These inputs were used because these signals after islanding are significantly different compared to that of grid-connected events. The neural network used for detection utilized self-organizing maps. Simulation results showed a maximum accuracy of 97.92%.

Bayesian Classifiers

Bayes theorem calculates the probability of a certain set point belonging to a class given its set of parameters. Bayes classifiers use the Bayes theorem to find out which class the inputs are most likely to belong to and classify accordingly. Najy et al. used the ESPRIT algorithm and Bayes classifier for islanding detection (Najy et al. 2011). ESPRIT was used to estimate the amplitude, damping factor, oscillation frequency and initial phase of transient voltage and frequency waveforms at the PCC. These parameters were used as inputs to train and test the Bayes classifier. The ESPRIT algorithm achieved its target by minimizing a specific cost function. Results showed a high classification accuracy of 99%. However, running ESPRIT constantly puts a high computational burden on the system. Also, the system has to know when the islanding will occur and run ESPRIT to detect it. Therefore, it is impractical for real-time systems (Matic-Cuka and Kezunovic 2014). Probabilistic Neural Networks have also been used for islanding detection (Lidula, Perera, and Rajapakse 2009). These networks are based on the integration of ANN and Bayes classifier Its structure is similar to that of ANN. However, each of its neurons use the Bayes theorem to calculate the probability of its input signal belonging to a certain category and relaying the information to the output layer. Energy of the frequency bands obtained through wavelet transform was used as inputs to the classifier. The technique showed an overall classification accuracy of 90%.

Decision Trees

Decision Tree (DT) algorithm has been extensively tested for islanding detection (El-Arroudi et al. 2007; Samantaray 2010; Dong, Lu, and Yang 2009). A DT is a sequential flowchart in which each decision node compares an input variable to a certain threshold. The tree converges to a conclusion of the event type by comparing the values of the system parameters with the thresholds. The construction of the DT and the threshold selection are based on the supplied data. Each branch of the tree represents the outcome of the comparison of the input parameter with the threshold and the terminal nodes of the tree, called leaves, represent classification of the event.

El-Arroudi et al. used a data-mining software package called the Classification and Regression Tree to construct the DT model for islanding detection (El-Arroudi et al. 2007). However, it showed a high misclassification rate of 16% for islanding events. Samantaray et al. proposed a DT

model using a data mining package called Insightful Miner (Samantaray 2010). It was initialized with 11 input parameters from which it eventually selected three parameters to construct the DT model. The DT model was transformed to a fuzzy rule base by comparing the inputs to fuzzy membership functions. Each fuzzy membership function (FMF) represents a two-dimensional rectangular space instead of just a constant number. The use of FMF results in 100% classification, even in presence of significant noise in the system.

Lidula et al. compared the performance of three different machine learning classifiers for islanding detection, namely ANN, DT and support vector machines (Lidula, Perera, and Rajapakse 2009). They used wavelet transform to decompose the transient current signals at the PCC into six frequency bands, known as wavelet co-efficients. The energy associated with each frequency band was used as input to the classifiers. DT resulted in the best classification rate. However, the datasets used for training had a highly biased class distribution, leading to very optimistic results. In addition, it used a sampling rate of 40 kHz, which is much higher than 2-5 kHz generally used by digital relays (Matic-Cuka and Kezunovic 2014).

Dong et al. proposed the use of C4.5 DT for islanding detection (Dong, Lu, and Yang 2009). This algorithm constructs the DT by selecting the parameters which contain the maximum information regarding islanding classification. Eight different parameters were selected as initial inputs to the algorithm from which the C4.5 decision tree algorithm selects the parameter combination which showed the least misclassification rate. For the tested scenarios, this technique showed no misclassification. Faqhruldin et al. further refined the technique using a classifier called the random forest classifier (Faqhruldin, El-Saadany, and Zeineldin 2014). This classifier makes use of several independent C4.5 DTs in parallel and uses majority vote of the DTs to decide islanding. The technique showed an overall accuracy of 99% after 4-fold cross-validation.

Support Vector Machines

Support vector machine (SVM) is another type of classifier which has been used in islanding detection (Lidula, Perera, and Rajapakse 2009; Matic-Cuka and Kezunovic 2014). During training, the algorithm maps the input space nonlinearly into a high-dimensional feature space which results in increased separation among the different classes, so that they can be distinguished easily. The algorithm constructs this high dimensional feature space using a technique called structural risk minimization, which minimizes the upper bound on the expected risk. SVM can work with small datasets and has only a few adjustable parameters. In (Lidula, Perera, and Rajapakse 2009), wavelet transform has been used to extract features from current signals which were fed to a SVM for is-

landing detection. However, wavelet transform is sensitive to noise which affects the performance of the classifier. Autoregressive modeling has also been used to extract features from voltage and current signals (Matic-Cuka and Kezunovic 2014). It is a spectral analysis technique similar to the fourier and discrete wavelet transforms, however it has the advantages of being less computationally expensive. The features extracted from the AR model were used to train the classifier. It was shown to be insensitive to non-islanding events while having a pretty good islanding classification rate of 98.94%. However, it can fail to detect islanding for real power mismatches over 40% and reactive power mismatches over 5%. Therefore, it was proposed as a backup to the OUV/OUF technique.

Remote Islanding Detection Techniques

Remote islanding detection techniques rely on communication between the DG sources, utility protection, and monitoring system. Figure 12 shows the different techniques classified in a taxonomy based on the method of communication. The different communication methods utilized for islanding detection are discussed in the following subsections.

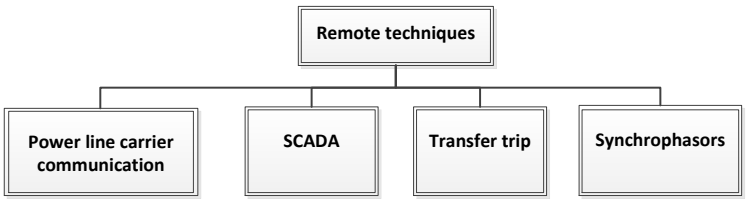

Figure 12. Taxonomy of remote islanding detection techniques

Power-Line Carrier Communication based Islanding Detection Technique

This technique monitors encoded signals sent remotely by the utility through the power line to confirm grid connection. If such a connection is lost, islanding is detected. Implementation of this technique requires the installation of transmitters on the utility side and receivers in every DG for proper operation. The frequency and the information content of the signal need to be selected based on various factors such as the attenuation of inductors to high frequency signals, possible customer replication of the signal, and so on (Ropp et al. 2000). The details of the design and implementation of such a technique were presented in (Wilsun Xu et al. 2007; Wang et al. 2007). This type of technique is very reliable but also very expensive to implement for small scale DG systems because of the high cost of transceivers required.

SCADA based Islanding Detection Technique

SCADA is a well-known acronym for Supervisory Control and Data Acquisition. The name represents an extensive communications and sensing network used by utilities to control and protect the power systems. In SCADA-based islanding detection techniques, voltage sensors are installed on the DG side which transmits the measurements back to the utility. If a voltage is detected on the disconnected DG side, alarm systems are triggered and corrective actions are taken (Bower and Ropp 2002). If the DG system is properly equipped with the required instrumentation for sensing and communication, this technique can effectively detect islanding. However, SCADA systems are generally not employed below the transmission level because of the substantial costs involved. High cost associated with implementing the communication infrastructure may not be justified for small DG systems.

Synchrophasor based Islanding Detection Technique

A synchrophasor, also known as a phasor measurement unit (PMU), is a device which sends synchronized voltage and current phasor data to the utility several times each second. Synchronization is done via a satellite based GPS. Having time-synchronized phasor data from several synchrophasors can help in wide-area protection and control (Sykes et al. 2007). Two different islanding detection methods have been proposed which utilize synchrophasor data. The first method is called the Angle Difference Method and is based on the difference between the local and remote voltage angle value (δ_k). At any instant k, δ_k is defined as follows:

$$\delta_k = \angle V_k^1 - \angle V_k^2 \tag{2.16}$$

where $\angle V_k^1$ and $\angle V_k^2$ are the phase angles of the positive voltage sequence measured by the PMUs at the DG and utility side respectively. When δ_k is greater than a predefined threshold for a certain period of time, islanding is detected.

The second method is known as the Acceleration-Slip Method. Slip and acceleration are the first and second order derivatives of δ_k respectively. During normal operation, both slip and acceleration have very small values (close to zero). During islanding, their absolute values tend to be much larger. This characteristic has been used to detect islanding. Pena et al. proposed an AI technique combining both of these methods with additional safeguards for false trips due to non-islanding events (Pena et al. 2013). Synchrophasor-based AI techniques can be very accurate and robust in islanding detection. However, the concept of synchrophasors is still relatively new.

Such devices are very expensive and are installed only in a handful of power systems. However, the number of PMUs installed is growing each year and islanding detection using synchrophasors will become popular.

Transfer Trip based Islanding Detection Technique

In the transfer trip scheme, the utility monitors and directly controls all the circuit breakers that can potentially island the DG (Mahat, Chen, and Bak-Jensen 2008; Massoud et al. 2009). During a disconnection, the scheme determines which areas are islanded and sends signals to all the islanded DGs to continue operation or to disconnect. This technique can be implemented into the existing SCADA system to monitor the status of the breakers and reclosers. It offers increased control and co-ordination of the DGs by the utility. However, with increased penetration of DG in the grid, the implementation and co-ordination of this technique becomes very complex and expensive.

Comparative Analysis of Existing Islanding Detection Techniques

There is no universal islanding technique that can work for all the different DG systems. Each technique has its advantages and disadvantages and the choice of implementation is a compromise between cost and desired reliability. Table 2 presents a comparative analysis of the conventional attributes of the different techniques.

Table 2. Comparison of existing islanding detection techniques

Technique	**NDZ**	**Detection Time**	**Power Quality**	**Cost**	**Detection Reliability**	**Effect of Multiple DGs**
Passive	Large	Short	No effect	Low	Low	None
Active	Small	Long	Degradation	Medium	High	Synchronization issues
Hybrid	Small	Long	Degradation	High	High	Synchronization issues
Machine Learning	Small	Variable	No effect	High	High	None
Remote	None	Very short	No effect	High	Very high	Increase in cost

Passive techniques are low-cost and scalable and can detect islanding with considerable power mismatch, which is the case in most scenarios. However, their performance depends on the selection of the threshold and settings which are too sensitive can lead to nuisance tripping. Active techniques have much smaller NDZ but they degrade the power quality under normal operation conditions. Loads with high Q_f can also cause performance issues when used with these tech-

niques. Another problem associated with active techniques is that high DG penetration can cause synchronization issues.

Hybrid techniques have very low NDZs and their power quality degradation is much smaller than active techniques because the active techniques are not applied continuously. However, they suffer from the drawback of having long detection time because the passive-active combination takes time to destabilize the island.

Machine learning techniques are generally very accurate in distinguishing between islanding and non-islanding events but they require extensive offline training. In addition, if the system topology changes, then they will have to be re-trained. Such investment of time and computing resources is not feasible for small DG systems. On the other hand, remote techniques are very reliable and have no NDZ but they are very expensive to implement, making them uneconomical for small DG systems.

Inspite of the large NDZ and nuisance tripping problem in passive techniques, they are widely implemented due to the ease in implementation of such techniques. Therefore, this thesis proposes two novel passive techniques which eliminate the problem of NDZ and nuisance tripping while maintaining the computational simplicity and low cost of conventional passive techniques. The methodology and performance of the techniques are presented in the following chapters.

Power Quality Event Detection and Classification

Unexpected variations in power system voltage or frequency can damage or shut down essential electrical equipments (Mahela, Shaik, and Gupta 2015). Therefore, the power quality (PQ) of the system is determined by the constancy in these parameters. Events which lead to deviation in the voltage or frequency waveforms are called PQ events. The detection and classification of PQ events helps provide a clear and smart understanding of the operational requirements to mitigate the effects of such events. Therefore, there has been extensive research regarding PQ event classification in recent years. IEEE Standard 1159 provides an extensive classification of the various types of PQ events (IEEE1159 2009). They are generally categorized as voltage or frequency events, based on which parameter shows deviations during the event. The most critical type of voltage events are voltage sags and swells. Short-circuit faults, induction motor starting and transformer energizing are some of the causes of voltage sags while voltage swells occur when a large load is disconnected. Other less critical voltage events such as harmonics, flicker and notching occur due to the operation of power electronics devices in the system. Frequency events can be oscillatory or non-oscillatory in nature. Oscillatory frequency events are generated due to wide area generator-interaction and are

used in modal analysis to determine the stability of the oscillation. Non-oscillatory frequency events occur when there is a substantial change in the load and generation balance in the power system. The remainder of this section provides a detailed literature review on the operating principles and results of the recently proposed classification techniques.

The event classification techniques generally select a set of parameters to be monitored for event detection. After occurrence of an event, features are extracted from the input parameters which can accurately represent the characteristics of the event to be used for classification. The most commonly used feature extraction techniques are transforms like wavelet transform and s-transform. These features are then used as inputs to classifiers which output the final classification decision. Machine learning algorithms such as DTs, ANNs, SVMs, etc have been extensively used as classifiers.

Eristi et al. classified various PQ events such as faults, line interruption, transformer energizing, etc. using three phase voltage signals as inputs (Eristi and Demir 2012). Wavelet transform was applied on the inputs to extract multi-resolution analysis co-efficients. The energy in these co-efficients were used as inputs to train SVM and ANN classifiers separately and their comparative performance was investigated. Results showed that SVM was better than ANN in classifying the events and could also be trained faster.

Chilukuri et al. applied s-transform on single phase voltage signals to obtain five different features such as amplitude factor, frequency factor, THD, standard deviation and means of s-contours (Chilukuri, Dash, and Basu 2004). Then a fuzzy-rule based algorithm was developed to classify events such as sags, swells, harmonics, line interruptions, flickers and other transients. A total of 340 events were simulated and the technique exhibited a 98% classification rate.

Samantaray classified PQ events such as voltage sags, swells, harmonics, frequency oscillations, etc using a combination of s-transform, DT, fuzzy logic (FL) and genetic algorithm (GA) (Samantaray 2010). Initially s-transform was applied on time domain samples of voltage of the PQ events to obtain frequency contours, magnitude-time and frequency-time plots. Then 4 features were extracted such as energy content of the frequency contour, standard deviation and variance of the s-matrix and auto-correlation. These features were then used by a DT to classify the events. The DT was then transformed to a fuzzy rule base using fuzzy membership functions. To simplify the fuzzy-rule base, GA was applied to tune the fuzzy model. Detailed comparative analysis with other classification techniques showed a significant improvement in classification accuracy.

Ray et al. also used s-transform to classify voltage sags and swells in grid-connected DG systems caused due to the variability in DG output, load change and grid impedance (Ray, Mohanty,

and Kishor 2013). S-transform was applied on the voltage signal to obtain ten different features. Modular probabilistic neural networks (MPNN), SVM and least square-support vector machines (LS-SVM) were the three tested classifiers. In MPNN, each module of probabilistic neural network was assigned to detect a single type of PQ disturbance. LS-SVM differs from conventional SVM in its selection of constraints and error variable and has a comparatively lesser computational complexity. Performance comparison of the three different techniques have been carried out using both MATLAB simulations and experimental verifications. Among the different classifiers, LS-SVM reported the highest accuracy of 98%.

Valtierra-Rodriguez et al. proposed a dual neural network technique for classification of a wide range of PQ events (Valtierra-Rodriguez et al. 2014). An adaptive linear network (ADALINE) using THD and RMS voltage amplitude information to detect harmonic, sag, swell and outages and a feedforward NN used vertical and horizontal histograms of a specific voltage waveform to classify flickers, spikes, oscillations, etc were proposed. This technique was also tested for a combination of events occurring simultaneously. The technique showed high accuracy and the immunity of ANNs to noise helped to achieve an average of 94% classification accuracy in noisy environments.

Reaz et al. used an Artificial Neural Network - Fuzzy Logic combination to classify various PQ events (Reaz et al. 2007). Discrete wavelet transform was used to extract wavelet coefficients from three phase voltage samples. The ANN block performed pattern recognition of the coefficients and the classification output of the ANN was the input to a fuzzy logic block to provide more accurate and robust classification. Results showed an average classification rate of 98.19%.

Chen at al. used principal component analysis and scatter-plot based event classification (SPEC) to classify voltage and frequency events recorded by PMUs (Chen, Le Xie, and Kumar 2014). PMUs record a large number of parameters at the point of installation such as bus frequency, voltage magnitude, voltage angle, etc. Therefore, principal component analysis was applied to reduce the dimensionality of the data by only selecting parameters from the PMU data which can accurately represent the system. Event classification was triggered when one of the selected parameters exceeded a predefined threshold. The event was classified by searching scatter topologies and matching the current topology with an existing one. However, extensive performance analysis of this technique was not presented and so there is no information about the level of accuracy of this technique.

Table 3 presents a comparison of the different event classification techniques discussed in this section.

The event classification technique proposed in this thesis focuses solely on classification of local events which have a substantial impact on the operation of grid-connected DG systems. Besides

Table 3. Comparison of existing event classification techniques

Reference	**Feature extraction**	**Classifier**	**Accuracy** (%)
Chilukuri 2004	S transform	Fuzzy rule	98
Reaz 2007	Discrete Wavelet Transform	ANN-FL combination	98.19
Samantaray 2010	S transform	DT, FL and GA	96-98
Eristi 2012	Wavelet transform	SVM and ANN	SVM: 98.51 ANN: 97.02
Ray 2013	S transform	MPNN, SVM, LS-SVM	MPNN:98 SVM: 98 LS-SVM: 98.33
Valtierra-Rodriguez 2014	Fourier transform	Dual Neural Networks	94-98
Chen 2014	Principal component analysis	Scatter plot correlation	Not reported

PQ events, it can also detect DG islanding and classify the type of mismatch in the island. To the best of the author's knowledge, this is the first work which incorporates islanding events in event classification. As more and more DGs are integrated into the power grid, such classification will become critical to devise solutions to mitigate the negative impacts of such events.

Chapter 3

TECHNICAL DETAILS OF THE PROPOSED TECHNIQUES

This chapter is divided into three sections. The first two sections are devoted to the description of the operating principles and methodology of the two proposed islanding detection techniques. The final section discusses the selected inputs, methodology and architecture of the DG event classification technique.

Voltage Amplitude based Islanding Detection

The output power of the DG inverter exhibits small variations due to the imperfections in its controller and harmonics generated due to high frequency inverter switching, dead time, and DC link voltage ripple (Matic-Cuka and Kezunovic 2014). This is shown in Figure 13.

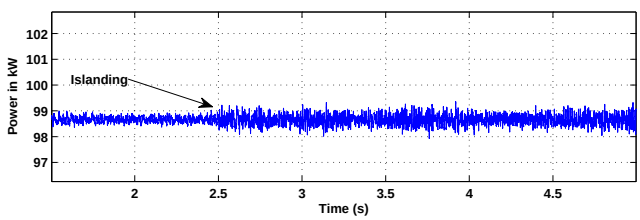

Figure 13. Output power of DG inverter

The low impedance grid absorbs these variations and thus the effect is not seen at the PCC voltage waveform. However, after the DG is islanded, the impact of these variations influence the voltage amplitude waveform. After islanding, the voltage amplitude at the PCC is calculated from (Jeraputra and Enjeti 2004),

$$\frac{V_i}{V} = \sqrt{\frac{P_i}{P_{Load}}} \tag{3.1}$$

Here V and V_i represent the local root mean square (RMS) value of grid connected and islanded voltage at PCC respectively. P_i and P_{Load} represent the output power of the inverter and the rated power consumed by the load. Since V and P_{Load} are constants, V_i depends solely on P_i. As a result, the variations in P_i are also reflected in V_i. This variation is always present in the waveform in an islanded condition. Other power system disturbances like short circuit faults, capacitor and load switching trigger a transient change in the voltage RMS level, but there are no sustained variations in figure 14 as seen in the islanded case, because of the stabilizing effect of the grid. Figure 14 shows the difference in the single phase RMS voltage waveforms for various

scenarios. Figure 14 (a) depicts a steady state grid connected scenario, showing negligible variations. Figure 14 (b) represents the islanded condition with zero real and reactive power mismatch, i.e., the power generated by the photovoltaic array (PV) is equal to the load demand of the island. This is considered to be the worst case scenario for conventional passive technique detection. Figure 14 (c) represents a severe three phase fault on a parallel feeder. The fault is cleared within two cycles by the circuit breaker on the feeder. As mentioned above, the waveform exhibits short transient spikes during initiation and clearance of faults.

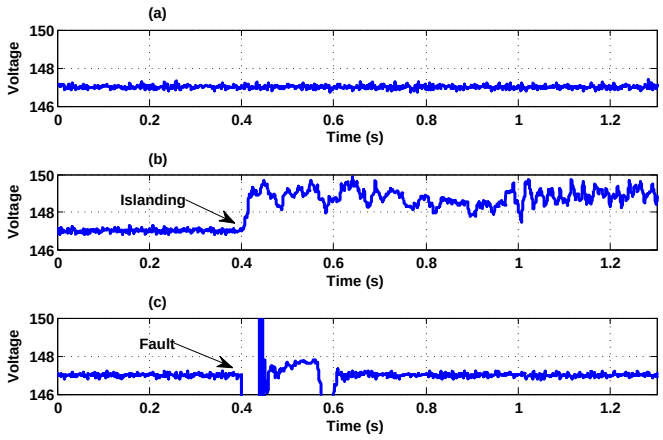

Figure 14. Root Mean Square (RMS) of single phase voltage waveforms at PCC for a) Grid-connected condition, b) islanding condition, c) three phase short circuit fault condition

The proposed islanding detection technique distinguishes islanding from non-islanding events by monitoring the ripple content patterns in the time domain RMS waveform of the PCC voltage. Figure 15 illustrates the proposed technique and figure 16 represents the input and output waveforms of each stage of the technique.

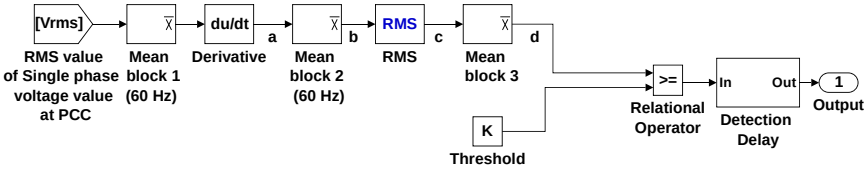

Figure 15. Proposed islanding detection technique block diagram

Stage 1 represents the single phase voltage (V) input at the PCC. Stage 2 displays the RMS value of V (V_{RMS}). The RMS is calculated over a running average window of one cycle of nominal system frequency (60 Hz). The equation for calculation of (V_{RMS}) is given in equation 3.2.

$$V_{RMS} = \sqrt{\frac{1}{T}\int_{t-T}^{t} V^2} \tag{3.2}$$

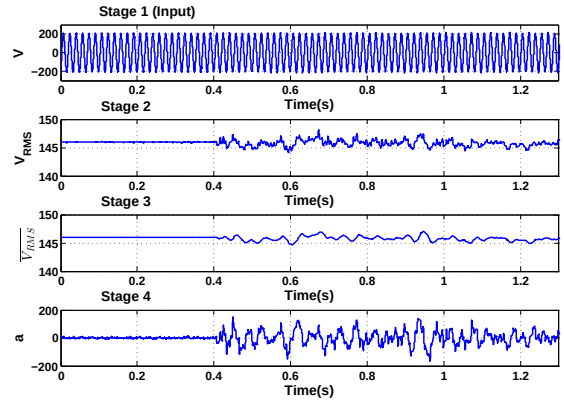

(a) Stages 1-4

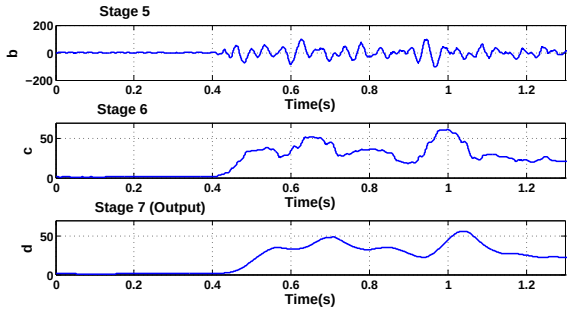

(b) Stages 5-7

Figure 16. Waveforms of all the stages of the islanding detection technique

where $T_{RMS} = \frac{1}{60}$ s.

The frequency components above 60 Hz in V_{RMS} act as noise for the technique and thus need to be eliminated. Therefore, the mean value of V_{RMS} is computed over a running average of one cycle of 60 Hz frequency. This has the same effect as a low-pass filter which eliminates any frequency component above 60 Hz. Stage 3 depicts the waveform for $\overline{V_{RMS}}$. The output of the filter is $\overline{V_{RMS}}$. The model of $\overline{V_{RMS}}$ is given in Equation 3.

$$\overline{V_{RMS}} = \frac{1}{T}\int_{t-T}^{t} V_{RMS}.dt \tag{3.3}$$

The changes in $\overline{V_{RMS}}$ are small and need to be amplified for the technique to work. This is achieved by taking the derivative of $\overline{V_{RMS}}$ to get a, as shown in equation 3.4. The derivative is calculated after each sample. The sampling time of the simulation is 10 μs. To further enhance the performance of the technique, the frequency components in a above 60 Hz were eliminated using another low-pass filter to get b, as shown in Stage 5.

$$a = \frac{d(\overline{V_{RMS}})}{dt} \tag{3.4}$$

$$b = \frac{1}{T}\int_{t-T}^{t} a \tag{3.5}$$

The RMS value of b was measured over a cycle of frequency (f_{RMS}) to get c, as shown in equation 3.6. This is achieved to quantify the ripple content and to eliminate any DC component present within b. Stage 6 shows the waveform for c.

$$c = \sqrt{\frac{1}{T_{RMS}}}\int_{t-T_{RMS}}^{t} b \tag{3.6}$$

Finally, any frequency component over f_{Mean} in c was eliminated to get the islanding detection waveform (d), shown in Stage 7.

$$d = \frac{1}{T_{Mean}}\int_{t-TMean}^{t} c \tag{3.7}$$

where $T_{RMS} = \frac{1}{f_{RMS}}$ s and $T_{Mean} = \frac{1}{f_{Mean}}$ s. The selection of f_{RMS} and f_{Mean} constitutes an important part of the technique design and is discussed in the next subsection. Figure 17 depicts the islanding detection waveform during normal operation, islanding and non-islanding conditions.

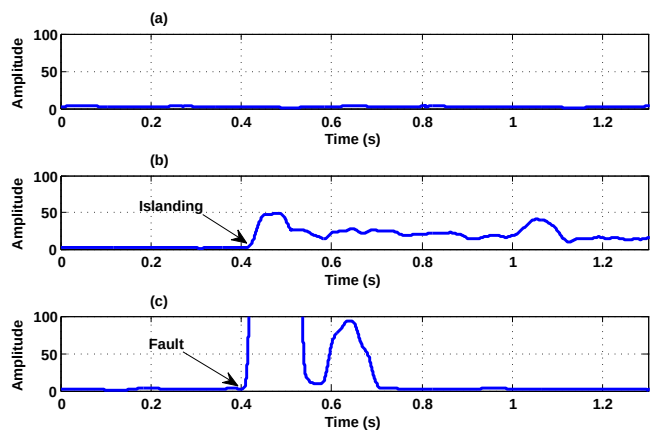

Figure 17. Islanding detection waveform. a) Grid-connected condition, b) islanding condition, c) three phase short circuit fault condition

In Figure 17, it can be noticed that for an islanding scenario, there is a substantial difference between the grid connected and the islanded level. For the fault scenario, although there is a transient spike in the waveform, it settles down relatively fast. Therefore, a certain threshold was used to differentiate between the grid connected and islanded waveforms. In addition, a time delay has been introduced in the detection to avoid any false trips due to transients caused by non-islanding scenarios like faults, load-switching or capacitance switching.

Let α be the selected detection threshold, t_d be the selected decision time delay, and Δt be the time interval in which d exceeds α. The islanding detection decision signal O_{ID_V} is,

$$O_{ID_V} = \begin{cases} 1 & if \;\; d \geq \alpha \;,\; \Delta t \geq t_d \\ 0 & if \;\; otherwise \end{cases} \tag{3.8}$$

where $O_{ID_V} = 1$ means islanding has been detected while $O_{ID_V} = 0$ means there is no islanding. Figure 18 depicts the algorithm for the proposed technique.

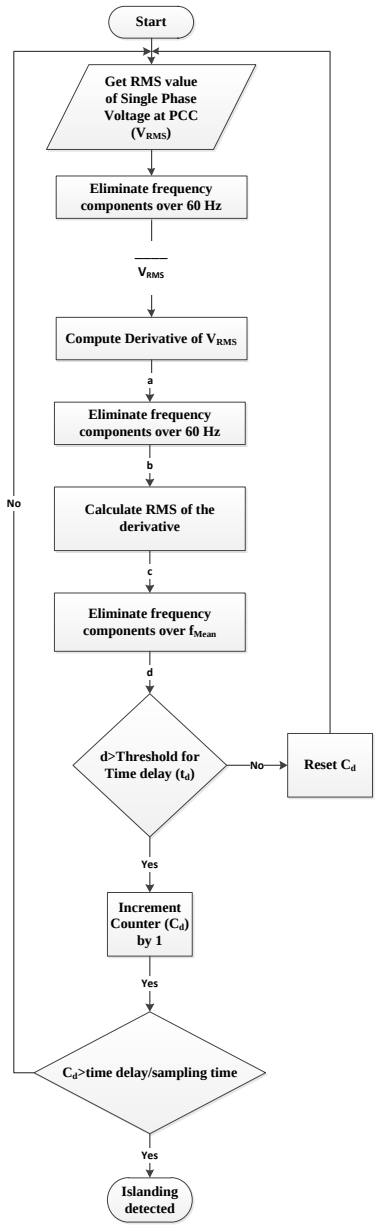

Figure 18. Algorithm for the detection technique

Model Parameter Optimization

The threshold and time delay for islanding detection were optimized based on thorough experimental analysis of possible islanding and non-islanding events. The factors affecting the selection procedure and the final selected values are given in this section.

The selection of the calculation frequency of the Mean 3 and RMS blocks, shown in Figure 15, is an important part of the design of the technique. The calculation frequency represents the time interval over which the RMS or mean calculation takes place. Figure 19 shows the effect of changing the frequency of the Mean 3 and the RMS block while figure 20 represents the change in the waveform when the frequencies of both the blocks are changed.

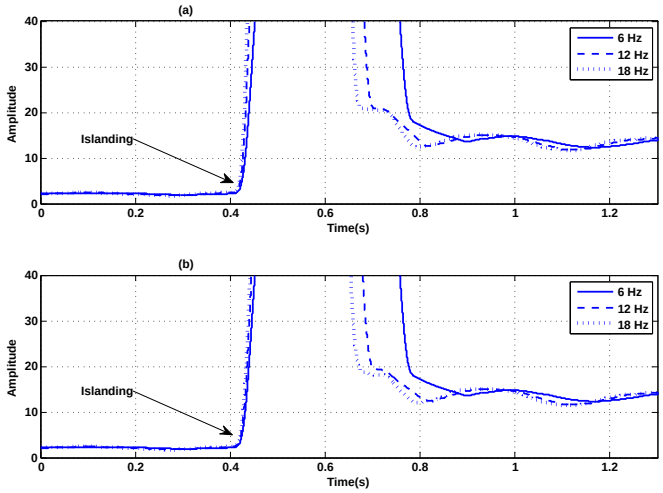

Figure 19. Effect of changing the fundamental frequency of (a) the Mean 3 block and (b) the RMS block on islanding detection waveform output

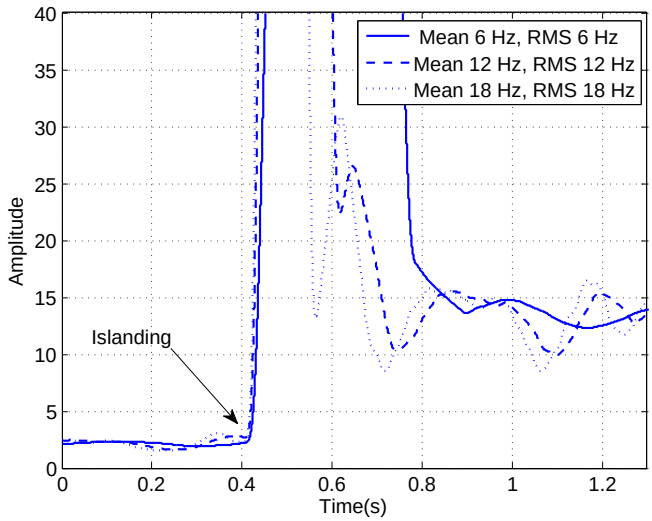

Figure 20. Effect of combined changing of the fundamental frequencies of the Mean 3 and RMS block on islanding detection waveform output

In both figures, it can be observed that there is no significant difference in the grid-connected waveform, but the difference in the islanded waveform is clearly visible. Although a low frequency helps in achieving a considerable difference between the grid-connected and islanded levels, it also has the effect of increasing the time it takes for the waveform to settle down to a stable value during other power system disturbances (e.g., faults, load switching, etc.). This is depicted in Figure 21.

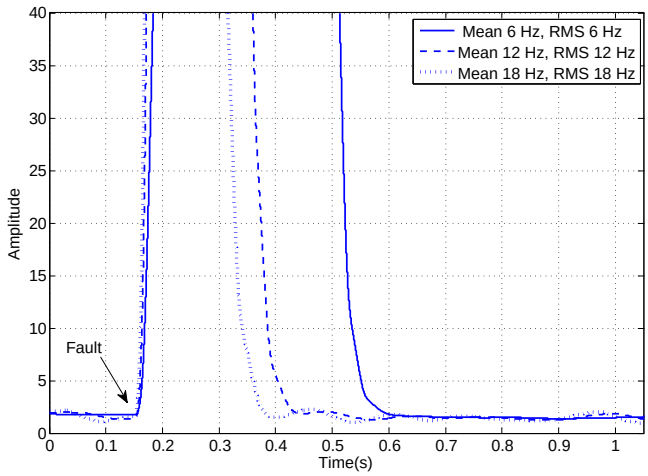

Figure 21. Effect of combined changing of the fundamental frequencies of the Mean 3 and RMS block on settling time delay after three phase fault

So, an optimum frequency for both the blocks had to be chosen so that there is adequate difference between the islanded and grid connected levels while the chosen delay is greater than the highest settling time recorded for non-islanding events.

The effect of changing the load quality factor (Q_f) on the detection waveform was also examined. Q_f is defined as the ratio of the reactive power consumption of the load to the rated power output of the DG inverter. IEEE standards require that the effectiveness of the islanding detection technique should be tested with loads having $1 \leq Q_f \leq 2.5$ at resonant frequency (Stevens et al. 2000). This means that the load behaves as a purely resistive load at 60 Hz, i.e., at this frequency, its inductive and capacitive power requirements cancel each other. Figure 22 shows the general effect of changing the Q_f on the output waveform. The case shown here is an island with zero mismatch and with both the mean 3 and RMS fundamental frequency set at 12 Hz. A higher quality factor reduces the margin between the islanding and non-islanding levels. This is because a higher Q_f means there is increased reactance in the load and high reactances obstruct any high frequency oscillations in voltage or current waveforms. The high reactance of the load decreases the amount of oscillations in the output voltage waveform amplitude after islanding. A similar effect is

seen in the output waveform for every other island scenario. So, the threshold was set based on the worst Q_f case.

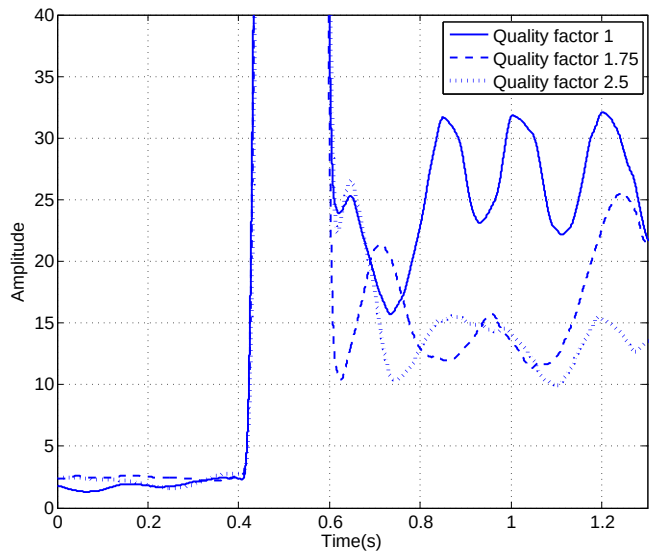

Figure 22. Effect of changing the load Q_f on islanding detection waveform output

After thorough experimentation with islanding and non-islanding events with fundamental frequencies of 6-30 Hz at quality factor of 2.5, the fundamental frequency of 12 Hz for both the Mean and RMS blocks were selected. The optimum threshold and time delay at this frequency were 4.5 V/s and 0.3 seconds respectively.

Rate of Change of Frequency based Islanding Detection

The increased distortions in V_{PCC} waveform after islanding due to DG inverter harmonics also lead to sustained variations in the frequency, thereby increasing the rate of change of frequency (ROCOF). Non-islanding events such as faults and capacitor switching can also cause transient spikes in the ROCOF waveform but usually they settle down within a short period of time. The difference between the ROCOF waveform for islanding and non-islanding events are illustrated in Figure 23.

Due to the observed variations, the ripple content in the ROCOF waveform has also been monitored and used to detect islanding whenever a predefined threshold is triggered. As shown in Figure 24, a 60 Hz low pass filter (LPF) with a cut-off frequency (f_c) is used to eliminate the noise in the ROCOF input. The ripple content in the ROCOF waveform is amplified by taking the instantaneous derivative of the filtered signal. After elimination of high frequency noise using a second LPF at the same f_c, the root mean square (RMS) of the resultant signal is measured to

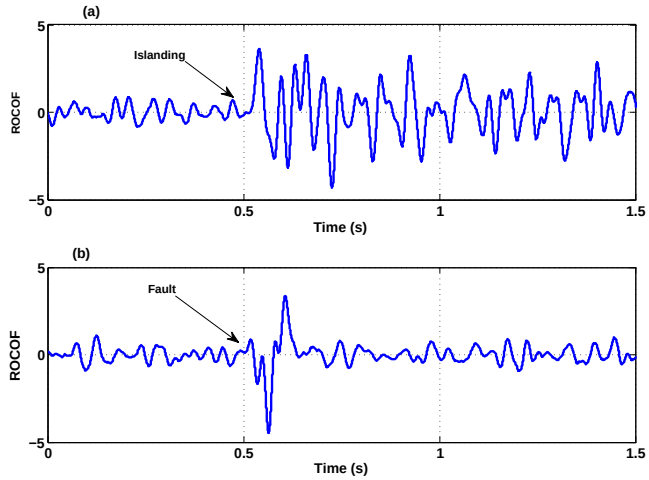

Figure 23. Variations in the ROCOF waveform during (a) Islanding event with zero power mismatch and (b) Three phase short circuit fault (non-islanding event)

quantify the ripple content and eliminate any DC component. The output of the RMS block is smoothed by a third LPF to obtain the desired islanding detection waveform (IDW).

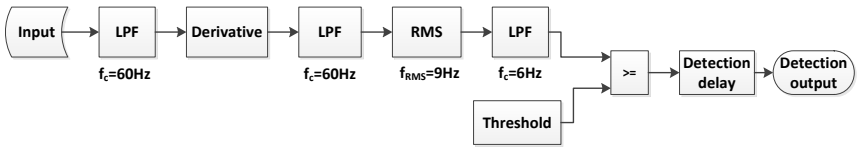

Figure 24. Block diagram of proposed detection technique

The relationships between the input ROCOF and IDW waveforms can be mathematically modeled as follows:

$$IDW = \overline{\left[\frac{\mathrm{d}\left(\overline{ROCOF}\right)}{\mathrm{d}t}\right]_{RMS}} \tag{3.9}$$

Let α be the selected threshold, t_d be the predefined detection delay, and Δt be the time delay during which IDW $> \alpha$. The detection signal $O_{ID_{ROCOF}}$ can be obtained as follows,

$$O_{ID_{ROCOF}} = \begin{cases} 1\ (islanding)\ \ if\ \ \ IDW \geq \alpha\ ,\ \Delta t \geq t_d \\ 0\ (non-islanding)\ \ if\ \ otherwise \end{cases} \tag{3.10}$$

Using model parameter optimization, a frequency of 9 Hz for the RMS block (f_{RMS}) and f_c of 6 Hz for the third LPF were selected. This resulted in a optimal IDW waveform from which threshold selection was convenient. Similar to the previous technique, the threshold and detection delay were chosen based on simulation results under islanding and non-islanding conditions for the worst Q_f condition. The IDW values for normal grid-connected operation are assumed to be under

$55Hz/s^2$. For islanding events, the minimum recorded value for IDW was $65Hz/s^2$, therefore, the threshold value (α) was set at $60Hz/s^2$. The maximum settling time recorded for non-islanding events was 280 ms, therefore t_d was chosen to be 300 ms.

DG Event Classification Using Artificial Neural Networks

Local power system events, such as islanding, faults, load switching, etc., have their own signature on the electrical measurements at the PCC of the DG. If detailed local electrical measurements are recorded for various events, distinct patterns can be observed in parameters such as voltage, frequency, etc. An example is illustrated in Figure 25 which consists of the voltage amplitude waveforms for different types of events over a period of ten cycles.

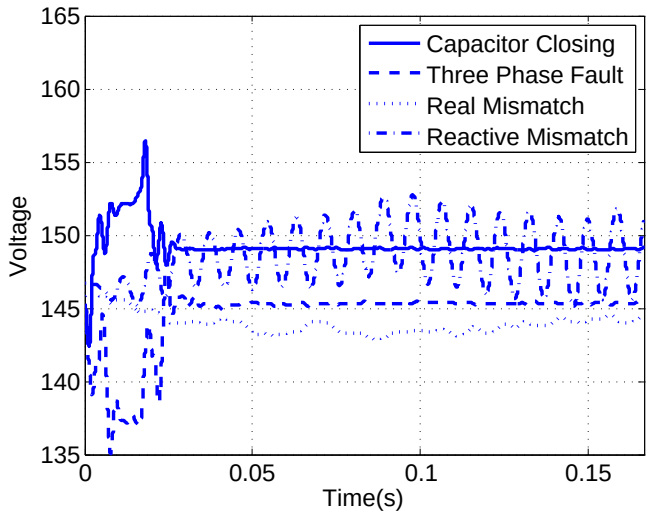

Figure 25. Waveforms of voltage amplitude for different event types

It can be observed from the figure that each event exhibits its own distinct pattern in the waveforms. On the other hand, events of the same type exhibit high correlation. This is observed in Figure 26 which shows the RMS voltage waveform for three phase faults of different magnitudes. Although the differences are visible in the waveform patterns, there is no definite model to distinguish between these events. Therefore, a suitable machine learning technique needs to be employed which can train itself to classify various local events by observing the pattern in selected parameters at the PCC. Artificial Neural Networks (ANN) were selected for this supervised pattern recognition challenge because they possess the ability to learn from complex non-linear input-output relationships and to adapt themselves to the given data (Basu, Bhattacharyya, and Kim 2010). Besides this, the training algorithms for ANNs are quite well established for use in

research. One of the most popular technique used for such a supervised pattern recognition challenge is the Feedforward ANN. The general architecture of a feedforward ANN is shown in Figure 27.

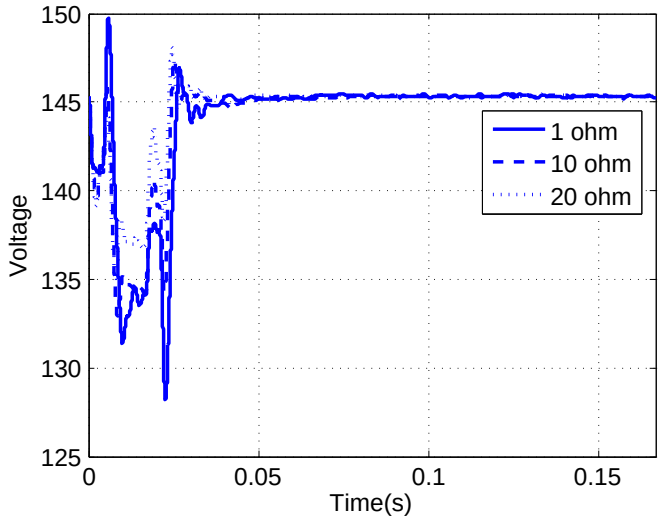

Figure 26. Waveforms of voltage amplitude for similar event types

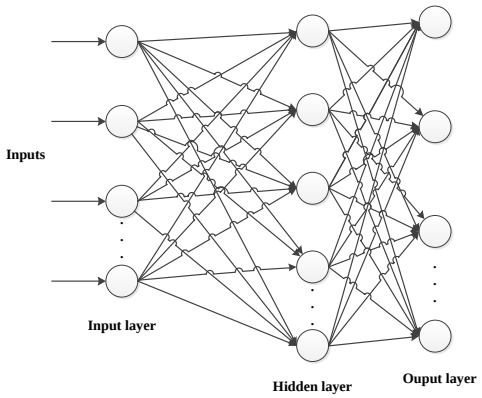

Figure 27. Structure of a feedforward neural network

This type of network is composed of several layers and each layer consists of multiple parallel nodes. The number of nodes in the input and output layers are equal to the number of input features and number of classes respectively. The layer between the input and output layers is called the hidden layer and the design of this layer is the most crucial part of network construction. The nodes in this layer are called neurons and they represent the fundamental building block of the ANN. Each neuron consists of inputs, scalar weights, a scalar bias and a transfer function. Figure 28 illustrates the general structure of a layer of neurons. The input vector I consists of inputs I_1 through I_k. Each element of this vector is associated to each neuron through the weight matrix W consisting of $r \times k$ elements, where r is the number of neurons in the layer. In the i-th neuron, all the weighted

inputs are added together alongwith the bias b_i to obtain n_i. n_i is then passed through a transfer function to get a_i. The relation between the final output of the neuron (a) and the input (I) is:

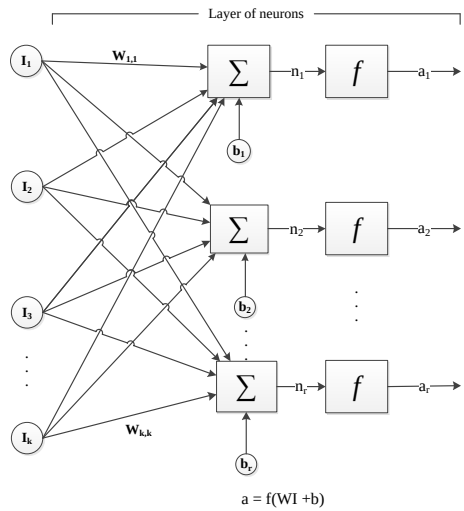

Figure 28. A layer of neurons in an Artificial Neural Network

At the beginning of ANN training, the weights and bias are initialized randomly. Then, in each iteration, the training algorithm changes the values of these parameters until the network response matches the desired response. This is generally done by continuously adjusting the weight matrix till its elements becomes small or the error function is minimized. The error function is dependent on the error in classification. The weights are adjusted according to the derivatives of the error functions with respect to the individual weights. The transfer functions serve the purpose of normalizing the input data because most training algorithms are sensitive to the scale of the data. The most popular transfer functions used for the hidden and output layers of ANNs are sigmoid functions mainly because they are easily differentiable (Isa et al. 2010).

The proposed DG event classification method consisted of three principal stages: parameter selection, feature extraction and model construction and optimization. In the parameter selection stage, the local current and voltage waveforms were measured and eight different local parameters were chosen as inputs for the classification technique. The input parameters selected for this purpose are listed in Table 4. The parameters selected had a high probability of showing patterns useful for classification of events.

Next, the feature extraction stage consisted of extracting a set of mean values from the input parameters. For each of the selected parameters, the mean values for each cycle, up to ten cycles, were recorded after the occurrence of an event. A separate matrix of data for each parameter was then constructed. The organization of this input matrix is depicted in Table 5. In it, $Mean_{ij}$

Table 4. Parameters selected for event classification

Parameter	**Symbol**
Voltage amplitude in pu	V_{pu}
Rate of change of voltage	$\frac{dV}{dt}$
Voltage total harmonic distortion	THD_V
Current total harmonic distortion	THD_I
Frequency in Hz	f
Rate of change of frequency	$\frac{df}{dt}$
Power factor	PF
Rate of change of power factor	$\frac{dPF}{dt}$

represents the mean value of the parameter for the i-th cycle after the occurrence of the j-th event. In the matrix, N represents the total number of samples. A separate neural network was then assigned to each matrix of data. The matrix helps the neural network reconstruct the pattern of the parameter over a period of ten cycles after the occurrence of an event.

Table 5. Organization of input matrix to neural networks

$Mean_{11}$	$Mean_{12}$	$Mean_{13}$	.....	$Mean_{1N}$
$Mean_{21}$	$Mean_{22}$	$Mean_{23}$	.....	$Mean_{2N}$
$Mean_{31}$	$Mean_{32}$	$Mean_{33}$	.....	$Mean_{3N}$
....	....	....	....	....
$Mean_{m1}$	$Mean_{m2}$	$Mean_{m3}$	.....	$Mean_{mN}$

In the model construction and optimization stage, the neural networks were trained with the help of MATLAB's Neural Network Toolbox. The pattern recognition feature of this toolbox was used for constructing the feedforward network. The hidden layers in the neural network are connected through tan-sigmoid transfer functions while the transfer function in the output layer is the softmax function. This combination of transfer functions is widely used for pattern recognition (Isa et al. 2010). The scaled conjugate gradient training algorithm was used because it is fast, memory efficient and is suitable for large complicated problems such as this one (Moller 1993). Table 6 lists the selected hidden and output layer transfer functions and the training algorithm for the ANNs and the reasons behind the selection.

The k-fold cross-validation method was used to train and validate the performance of each neural network. In this method, the dataset was divided into k subsets containing equal numbers of the different types of events. Then, (k-1) subsets are used to train the network and the validation

Table 6. Details regarding ANN transfer function and training algorithm selection

Design Parameter	Selection choice	Reasons for selection
Transfer functions	Tan-sigmoid (hidden layer) Softmax (output layer)	- Normalize inputs - Highly differentiable
Training algorithm	Scaled conjugate gradient	- Fast training - Memory efficient - Suitable for complicated problems

is conducted using the remaining subset. The process is repeated k times and the average misclassification rate was recorded as the performance index. The number of neurons in the hidden layer of each network was changed from 1 to 20 and the cross-validation method was repeated in every step. The selection of the number of neurons for each network was based on the optimal validation performance.

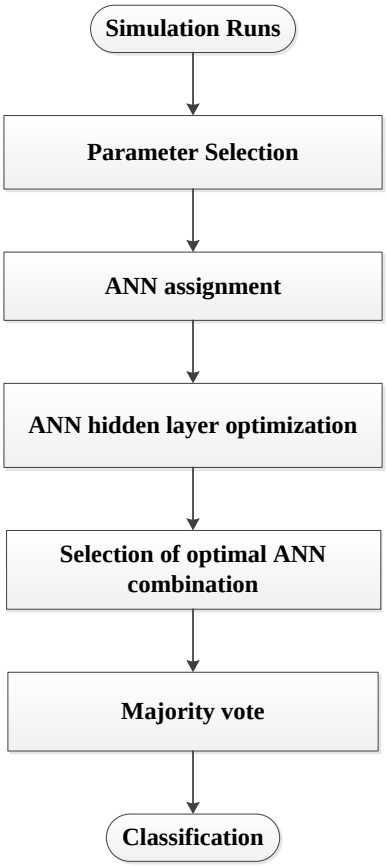

Figure 29. Proposed approach for DG event classification

After the optimization of each neural network, the outputs from each network was arranged in a vector and the majority vote of all the neural networks was selected as the final classification

output. This is done to provide more accurate and robust results compared to a neural network which is based on a single parameter only. However, combining 8 separate ANNs together also makes the event classification technique quite computationally complex. To decrease the computational complexity of the technique, the input parameters with low classification accuracy were eliminated one by one till an optimal classification performance was achieved. In each step, the parameter having the lowest accuracy was eliminated and the updated classification performance was recorded. The process stopped when further elimination led to a decrease in the performance. Figure 29 summarizes the methodology of the proposed DG event classification technique.

Chapter 4

RESULTS AND PERFORMANCE ANALYSIS

The performance of the proposed techniques has been investigated using a grid-connected PV system modeled in a MATLAB/Simulink environment as shown in figure 30 (a).

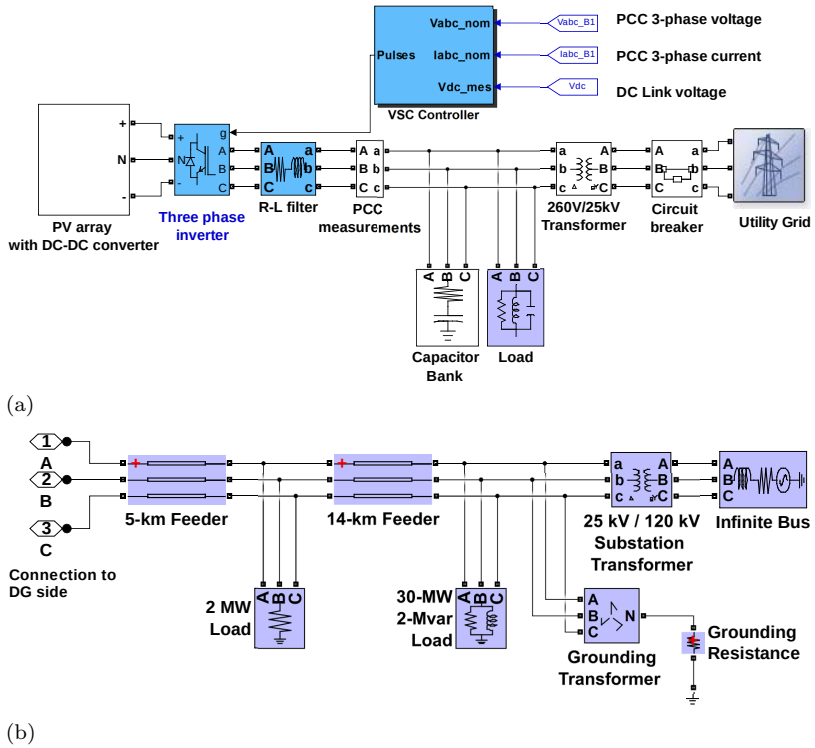

Figure 30. Simulink models of (a) DG System. (b) Utility grid

System specifications are listed in table 7. The PV model simulated the characteristics of SunPower (SPR-305) modules. The open-circuit voltage and short-circuit current of each module were 64.2 V and 5.96 A respectively. The PV array consisted of 66 strings of 5 series-connected modules in parallel to produce rated power at 1000 W/m^2 irradiance and 25^oC ambient temperature. It was connected to a DC-DC converter with switching duty cycle controlled by a Maximum Power Point Tracking (MPPT) controller. The purpose of the MPPT controller, as its name indicates, is to extract the maximum power from the PV as irradiance and temperature vary. The MPPT controller was implemented using the Incremental Conductance and Integral Regulator technique. The converter was connected to a 3-phase inverter to convert DC into AC and to synchronize with the grid. The inverter was programmed to output constant power at unity power factor. The load was connected as a parallel RLC circuit with constant impedance. Load quality factor (Q_f) was selected to be 2.5 and resonant frequency was set at 60 Hz to simulate the worst case scenario defined

Table 7. Specifications of the simulation model

Parameter	Value
PV array rated power output	100 kW
Load quality factor (Q_f)	2.5
Load resonant frequency	60 Hz
Inverter switching frequency	1980 Hz
Filter resistance	2 mΩ
Filter inductance	0.2 mH
Transformer nominal power	150 kVA
Infinite bus short circuit MVA	2500
Infinite bus voltage	120 kV

by IEEE 1547 (IEEE1547 2009) and UL 1741 (UL1741 2001) interconnection standards. The output voltage of the inverter was 260 V and it was connected to the grid via a step-up transformer. The RL filter and capacitor bank were used to filter harmonics produced by the inverter and also to provide reactive power. The 3-phase circuit breaker on the utility side was switched open in order to simulate the occurrence of islanding. The utility grid model shown in figure 30 (b) consisted of a 25 kV distribution feeder and a 120 kV equivalent transmission system. The distribution feeder is connected to two large loads ([2 MW], [30 MW, 2 MVAR]) and a 120 kV infinite bus via the substation transformer.

Results of Voltage Amplitude based Islanding Detection Technique

A large number of possible islanding and non-islanding events were simulated to verify the performance of the voltage amplitude detection technique. Table 8 lists all the different types of simulated events and the number of cases simulated for each event.

Results of Islanding Events

Figure 31 shows the results obtained for an island with zero power mismatch. Figure 31 (a) and (b) show the islanding detection waveform and output signal of the technique respectively. Before islanding, the waveform stays well below the predefined threshold. After islanding, the waveform consistently stays above the threshold and so islanding is detected after approximately 0.3 seconds.

Both positive and negative real power mismatch scenarios were simulated at a Q_f of 2.5 and with 1% increments from 1 to 10% and then 10% increments from 20 to 50%. Positive real power mismatch means that the generator supplies more power than what the load consumes and similarly negative real power mismatch means the load consumes more power than what the generator can

Table 8. Islanding and non-islanding scenarios simulated

Event	**Classification**	**Parameter Range**	**No. of Events**
Real Power Mismatch	Islanding	-50 to +50	29
Reactive Power Mismatch	Islanding	-4 to +4	8
Three-Phase Faults	Non-Islanding	1-75Ω Fault Resistance	25
Line-to-Line Faults	Non-Islanding	1-75Ω Fault Resistance	25
Single-Phase Faults	Non-Islanding	1-75Ω Fault Resistance	25
Load Switching in 260 V side	Non-Islanding	10-100 kVA	10
Load Switching in 25 kV side	Non-Islanding	1-30 MVA	10
Capacitor Switching in 260 V side	Non-Islanding	3-30 kVAR	10
Capacitor Switching in 25 kV side	Non-Islanding	300-3000 kVAR	10
Loss of Parallel Feeder	Non-Islanding	100-2000 MVA_{sc}	20
Motor Starting	Non-Islanding	100-300 kVA	20

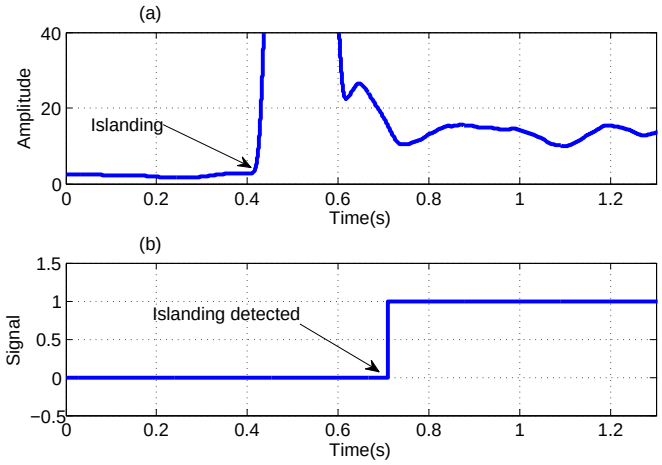

Figure 31. Results for zero mismatch scenario. (a) Islanding detection waveform. (b) Islanding detection signal

supply. The percentage is with respect to the nominal load real power. Figure 32 shows the waveform and the detection for $\pm$10% and $\pm$20% real power mismatch. P_L represents the load real power. The waveforms never go below the predefined threshold after islanding and this results in accurate detection every time.

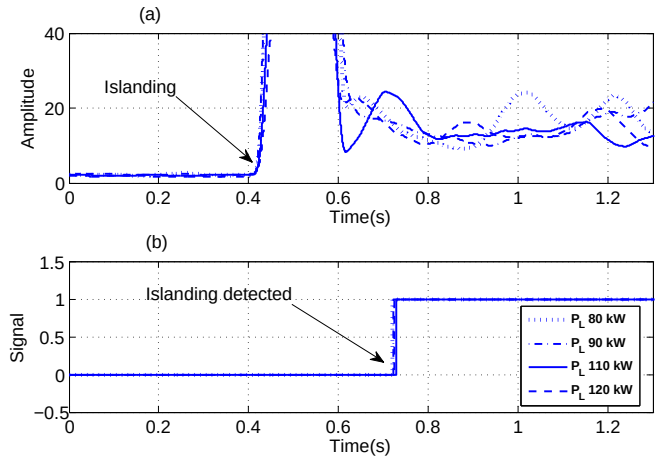

Figure 32. Results for real power mismatch scenarios. (a) Islanding detection waveform. (b) Islanding trigger signal

Reactive mismatch scenarios upto $\pm$4% were simulated with Q_f equal to 2.5. Here, positive reactive mismatch means that the inductive power requirement of the load is greater than its capacitive requirement and negative means the opposite. Figure 33 shows the waveform and detection for $\pm$1% and $\pm$4% reactive power mismatch. ΔQ_L represents the percentage reactive power mismatch. Similar to other islanding scenarios, the waveforms stay well above the threshold, resulting in detection. It is also observed that the minimum level of the islanded waveform is higher for higher levels of reactive mismatch. As a result, simulations of higher levels of reactive mismatch were not necessary for verification.

Results of Non-Islanding Events

The various possible non-islanding events which might falsely trigger an islanding detection technique are short circuit faults, loss of a parallel feeder (LOPF), load switching, capacitor switching, presence of non-linear load and starting of an large motor. Each of these techniques have been simulated to verify the accuracy of the technique.

Figures 34 and 35 show the waveforms for several of the non-islanding events simulated. The fault scenarios were simulated by initializing a short circuit fault on a parallel feeder. The circuit breaker on the parallel feeder tripped the feeder within 0.02 seconds, thereby clearing the fault. The type of short circuit faults simulated were three phase faults, line to line faults and single

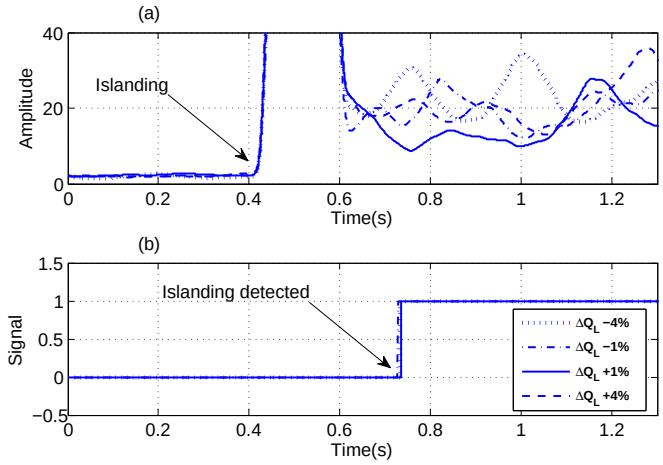

Figure 33. Results for reactive power mismatch scenarios. (a) Islanding detection waveform. (b) Islanding trigger signal

line to ground faults. For each type of fault, the total fault resistance was changed from 1Ω to 75Ω, with 3Ω increments. The fault scenario in figure 34 represents a 1Ω three phase fault occuring at 0.2 seconds.

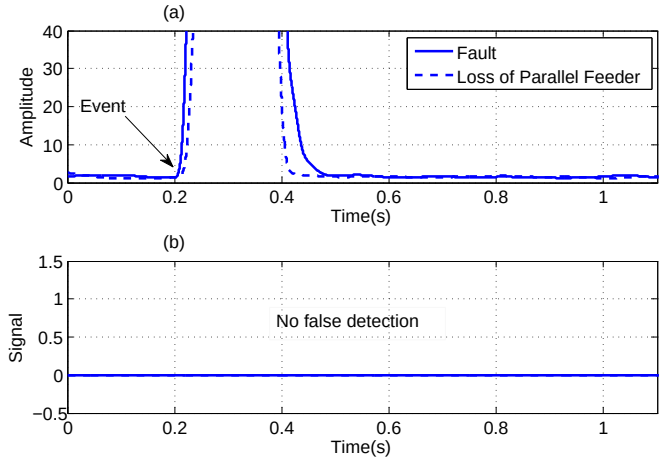

Figure 34. Results for fault and loss of parallel feeder. (a) Islanding detection waveform. (b) Islanding trigger signal

Simulations of LOPF were conducted too. In these simulations, the utility supply has been represented by two parallel feeders of equal short circuit strength. The total short circuit MVA of the feeders have been changed from 100 MVAsc to 2000 MVAsc with 100 MVAsc increments. The LOPF scenario in figure 34 represents a weak grid of 100 MVAsc, consisting of two parallel feeders of 50 MVAsc each. At 0.2 seconds, one of the feeders is disconnected to simulate LOPF.

Loads were switched in and out of the system on both the 260 V and the 25 kV side. On the 260 V side, the load kVA was changed from 10-100 kVA with 10 kVA increments. On the 25 kV

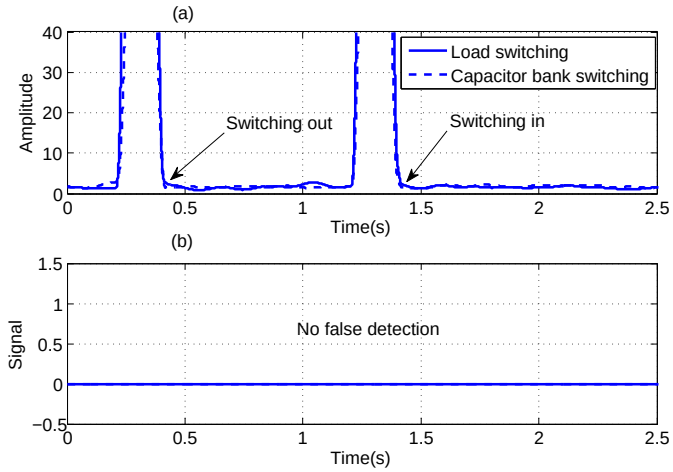

Figure 35. Results for load and capacitor bank switching (a) Islanding detection waveform. (b) Islanding detection signal

side, the load was changed from 1-30 MVA with 3 MVA increments. The load switching scenario in figure 35 represents the switching in and out of a 30 MVA load on the 25 kV side.

Switching in and out capacitor banks were also tested. In these simulations, the load was replaced with a capacitor. On the 260 V side, the capacitor ratings were varied between 3-30 kVAR, with 3 kVAR increments. On the 25 kV side, capacitor ratings were varied between 300-3000 kVAR with 300 kVAR increments. The capacitor bank switching scenario in figure 35 represents the switching in and out of a 3000 kVAR capacitor bank on the 25 kV side.

Table 9 shows the maximum time it took for the waveform to settle down for each of the above-mentioned non-islanding events. As can be observed from the table and the detection signals in figures 34 and 35, none of the events trigger false detection because the settling time for all the events were lower than the chosen detection delay for the technique.

Table 9. Maximum time delays for various non-islanding events

Event	**Maximum time delay (sec)**
Faults	0.2614
Capacitor switching	0.2075
Load switching	0.2037
Loss of parallel feeder	0.1995

A motor starting scenario can cause voltage variations in the system and this may falsely trigger the technique. Therefore, the effect of motor starting on the technique was tested and the test setup is illustrated in figure 36. The motor loading was changed to different values and the effect on the detection waveform was observed. In figure 37, the variations and oscillations in the PCC RMS Voltage waveforms are due to the high starting currents drawn by the motor. It has the

effect of causing two subsequent peaks in the detection waveform. As the motor power requirement goes up, the time it takes for the peaks to settle down keeps on increasing. As a result, the technique falsely detects islanding for motor loads beyond 245 kVA (328 HP), because the settling time exceeds 0.3 seconds. If the delay is extended, then the technique will also work for higher motor ratings as well. However, motor ratings above 300 HP are not very popular and so the delay was not changed to a higher value, to provide for fast islanding detection (Miller 1952).

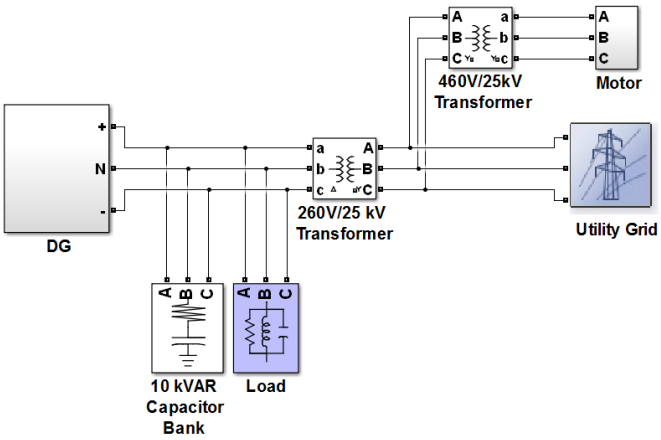

Figure 36. Setup to test the effect of starting an industrial motor

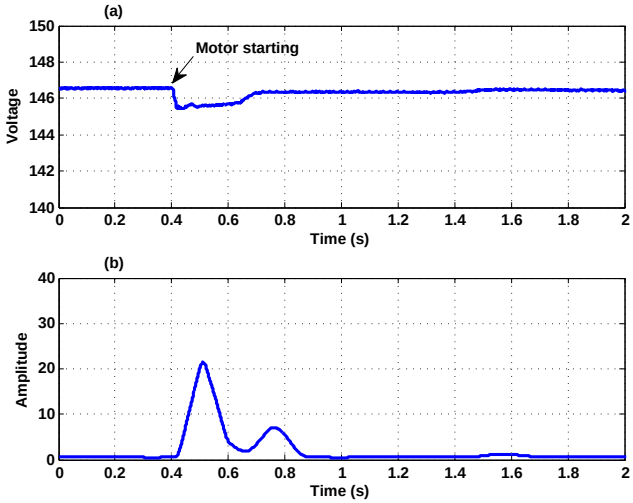

Figure 37. Effect of 100 kVA motor starting on (a) RMS Voltage waveform at PCC (b) Islanding detection waveform

Effect of various system parameters on performance of the technique

Several additional experiments related to the power system topology and parameters were conducted to verify the robustness of the technique. This subsection presents the results obtained from these experiments.

The impact of changing the DG nominal power on the detection technique was also tested. The rated output of the DG inverter and the peak power of the PV array were also varied between 25 to 200 kW with 25 kW increments. Table 10 lists the average grid connected and islanded values of the detection waveform for the different levels of DG nominal power.

Table 10. Effect of change of DG nominal power

DG nominal power (kW)	**Average before islanding** (V/s)	**Average after islanding**(V/s)
25	3.995	24.702
50	2.344	17.163
75	2.50614	14.407
100	1.95	15.67
125	1.778	13.782
150	1.826	18.961
175	2.738	15.145
200	3.834	42.560

The island scenario is that of a zero real power mismatch with a load Q_F of 2.5. This scenario was tested because it was the hardest islanding condition to detect. The grid-connected values of the detection waveform were always below the threshold and the islanded levels were always above it. This verifies that the performance of the technique is not limited to any scale of the systems.

The impact of the presence of multiple DGs on the performance of the technique was also investigated. Figure 38 illustrates the multiple DG model.

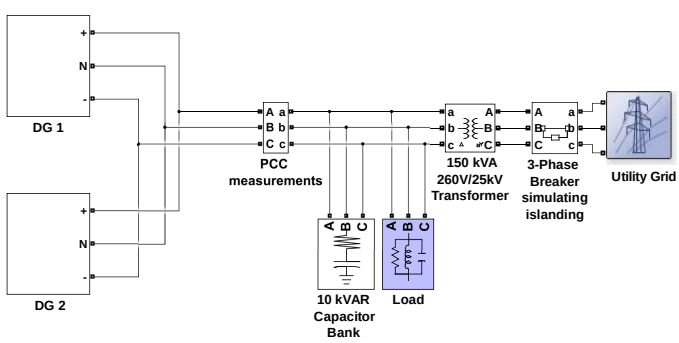

Figure 38. Model containing two DGs in parallel

In figure 38, both DGs were 100 kW PV systems, each having its own DC-DC converter, inverter and control systems. Three different islanding scenarios were simulated with load quality factor of 2.5. Table 11 lists the minimum (d_{min}) and maximum (d_{max}) levels of the detection waveform for both the single and double DG case.

Table 11. Comparison between values obtained from single and double DG simulations

Event	**Single DG case**		**Double DG case**	
	d_{min} (V/s)	d_{max} (V/s)	d_{min} (V/s)	d_{max} (V/s)
Zero mismatch	1.94	11.50	1.90	11.22
Real power deficit of 10%	1.76	13.21	2.51	10.13
Real power excess of 10%	2.20	9.92	1.92	9.94

It is observed that the values are quite close to each other. This proves that the performance of the technique is not affected by the presence of multiple DGs within the island.

Results of ROCOF based Islanding Detection Technique

To verify the performance of the technique, a wide range of islanding and non-islanding events were simulated, as shown in figure 39. The waveforms and detection signal for each of the simulated conditions are depicted in figure 40 through figure 43. IDW waveform is plotted in per unit values with α as the base value.

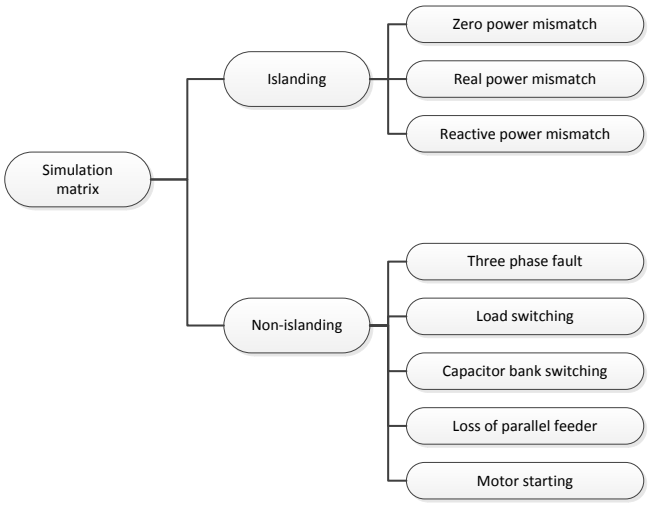

Figure 39. Taxonomy of islanding and non-Islanding Simulated Events

Results of Islanding Events

All the simulated islanding cases were chosen to lie within the NDZ of the OUV/OUF techniques currently used for islanding protection in modern PV inverters. According to IEEE 1547 and UL 1741 regulations, OUV/OUF protection should not trip the system when the voltage and frequency are within $88\% \leq V \leq 110\%$ and $59.3Hz \leq f \leq 60.5Hz$ respectively. For these bounds, the percentage range of real (ΔP) and reactive (ΔQ) power mismatch not leading to islanding detection

are given in equations 4.1 and 4.2 respectively (Zhihong et al. 2004). In these equations, P is the inverter rated power output.

$$-17.36\% \leq \frac{\Delta P}{P} \leq 29.13\% \tag{4.1}$$

$$-5.94\% \leq \frac{\Delta Q}{P} \leq 4.11\% \tag{4.2}$$

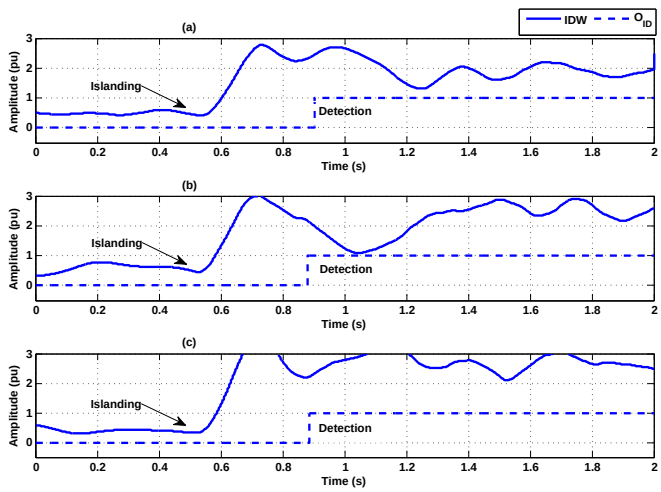

Figure 40. IDW and $O_{detection}$ for a) Zero mismatch b) 25% real power deficit c) 1% reactive power deficit

Positive (+) and negative (-) values for real and reactive power indicate scenarios where there is a deficit (-) or excess (+) in the power mismatch. For verification purposes, the simulated power mismatch for islanding events were $-20\% \leq$ Real power mismatch $\leq 30\%$ and $-6\% \leq$ Reactive power mismatch $\leq 6\%$. The plots for IDW and O_{ID} for 3 different islanding events are illustrated in figure 40. As indicated, islanding occurred at 0.5 s. Figure 40 (a) represents the zero power mismatch condition which is considered the hardest to detect. Thus, the proposed technique was able to successfully detect islanding within 400 ms. Figure 40 (b) represents a real power deficit of 25% which was also detected within 400 ms. After islanding, IDW almost reaches the threshold (α) for a very short period of time but never goes below it. Therefore, successful detection of islanding is once again observed. Figure 40 (c) shows 1% positive reactive mismatch condition. It is observed that IDW stays well above α after islanding resulting in successful islanding detection.

The effect of changing the generating capacity of the DG unit was also investigated. Figure 41 shows the IDW for a zero mismatch islanding case with different DG capacities of 50 kW, 100 kW, and 150 kW. In the grid-connected mode, the IDWs were almost similar in all scenarios. In islanded mode, although the waveforms look different, their minimum levels were very close to

each other and significantly above the predefined threshold. Similar patterns were observed for other islanded scenarios. Therefore, the technique's performance is not dependent on the DG capacity.

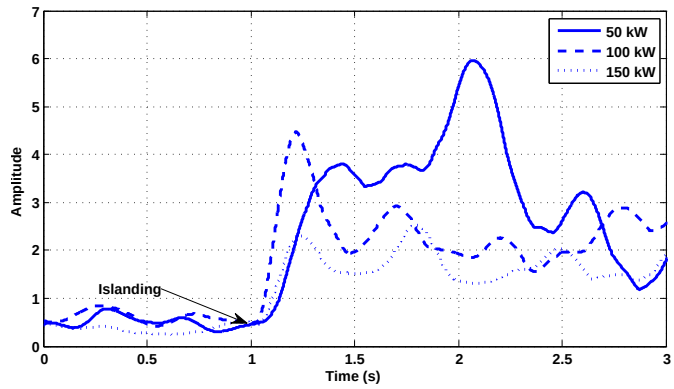

Figure 41. IDW for islanding with zero mismatch for different DG capacities

Results of Non-Islanding Events

In this section, the response of the proposed technique to non-islanding events is presented. The selected non-islanding events were known to cause nuisance trips in passive detection techniques. Figure 42 (a) depicts the IDW responses for a load switching scheme. A large load (100 MW, 50 MVAR) connected on the utility side was switched OFF at 0.5 s and switched ON at 2 s. Both of these events are known to trigger transient spikes in the inverter frequency which is reflected in the IDW waveform. However, these spikes settled down within the time delay (300 ms), therefore no false islanding was detected.

Figure 42 (b) shows the IDW waveform for switching a large capacitor bank connected to the 25 kV side and rated at 3 MVAR. Similar to the previous event, the capacitor bank is switched OFF at 0.5 s and back ON at 2 s. In both events, the IDW exhibited sharp peaks for less than 250 ms. The proposed technique did not falsely detect islanding since the settling time was less than the allowable time delay t_d.

In addition, short-circuit faults were also simulated both on the utility side and on the DG side for single line-to-ground, line-to-line, and 3-phase faults. It was observed that among all the non-islanding events, the 3-phase faults had the largest IDW oscillation settling time.

Figure 43 (a) shows the IDW waveform for a severe 3-phase fault occurring on the utility side with a very low fault resistance (1Ω). As shown, the transient spike falls below the threshold (α) for only 200 ms with no effect on the detection signal. The loss of parallel feeders is another non-islanding scenario affecting the frequency of the inverter. In this event, the grid short-circuit MVA was set at 500 MVA_{sc}. Figure 43 (b) shows the IDW signal for loss of parallel feeder. At 0.5

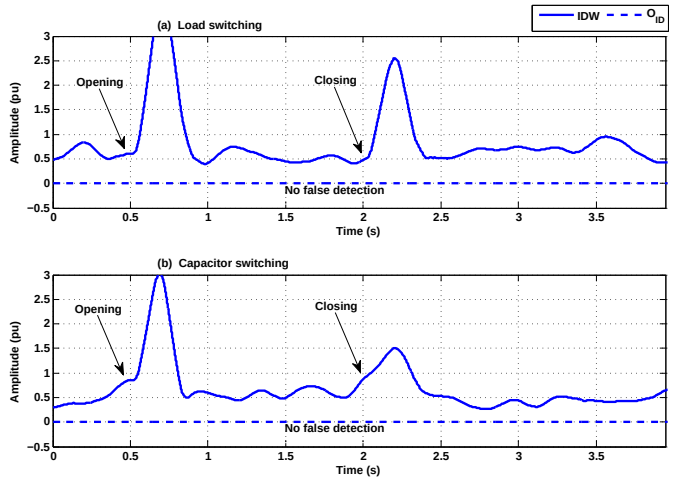

Figure 42. IDW and $O_{detection}$ for different switching events

s, the grid MVA_{sc} value dropped to 250 indicating the loss of a parallel feeder resulting in a 260 ms transient spike with no false islanding detection.

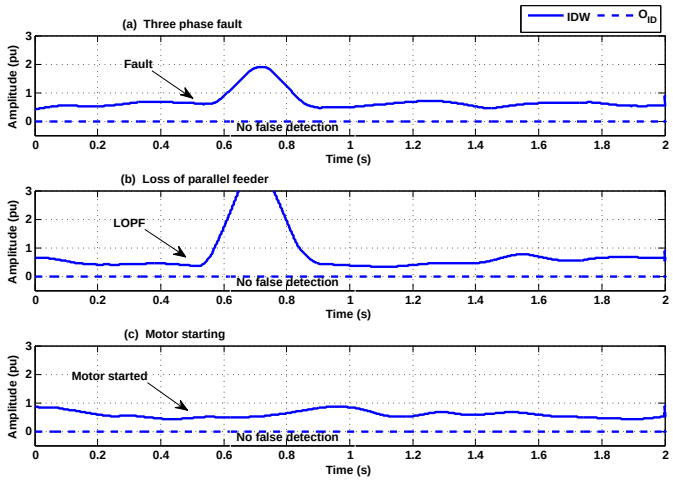

Figure 43. IDW and $O_{detection}$ for (a) Three phase fault (b) Loss of parallel feeder (c) Motor starting

The final simulated non-islanding event was the starting of a 460V, 300 kVA induction motor. The motor was connected to the utility through a transformer and it was turned on at 0.5 s. Although starting such a large motor draws high currents, it seems to have negligible effects on the frequency as shown in figure 43. The waveform did not even approach the threshold level when the motor started, therefore islanding was not falsely detected.

Results of ANN-based DG Event Classification Technique

The simulation model presented in the beginning of this chapter has been used for verification of the classification performance of the technique. A total of 310 events were simulated for training and

testing of the different ANNs. The distribution of the different types of events in the input samples is given in table 12.

Table 12. Simulated cases for DG event classification

Event	**Parameter Range**	**No. of Events**
Real Power Mismatch (Islanding)	-50% to +50% mismatch	30
Reactive Power Mismatch (Islanding)	-10% to +10% mismatch	30
Three-Phase Faults	1-60Ω fault resistance	30
Line-to-Line Faults	1-60Ω fault resistance	30
Single-Phase Faults	1-60Ω fault resistance	30
Load Closing Events	1-100 MVA load	30
Load Opening Events	1-100 MVA load	30
Capacitor Closing Events	250-3000 kVAR capacitor	30
Capacitor Opening Events	250-3000 kVAR capacitor	30
Loss of Parallel Feeder	1500-3500 MVA_{sc} infinite bus	30
Normal operation	50% to +150% of DG capacity	10

To make the distribution uniform, each type of event had 30 samples. 10 sample cases of grid-connected normal operation were also included in the input data so that the technique can operate in real-time. 10-fold cross-validation was conducted to evaluate the average performance of the ANNs. Each subset of data in the folds had equal distribution of the various types of events to avoid any bias in the training and testing.

Initially, all 8 parameters mentioned in chapter 3 were used as inputs to 8 ANNs (one ANN per parameter). Figure 44 depicts the change in the misclassification rate of two different ANNs (having V_{pu} and f as inputs) due to the change in the number of neurons in the hidden layer.

Table 13. Optimized classification performance of various ANNs

Input Parameter	**Optimal Neuron Number (n)**	**Optimized Accuracy(%)**
V_{pu}	12	97.10
f	20	93.55
$\frac{df}{dt}$	16	91.29
$\frac{dV}{dt}$	17	86.78
THD_V	7	85.16
THD_I	20	79.03
PF	15	68.39
$\frac{dPF}{dt}$	4	66.13

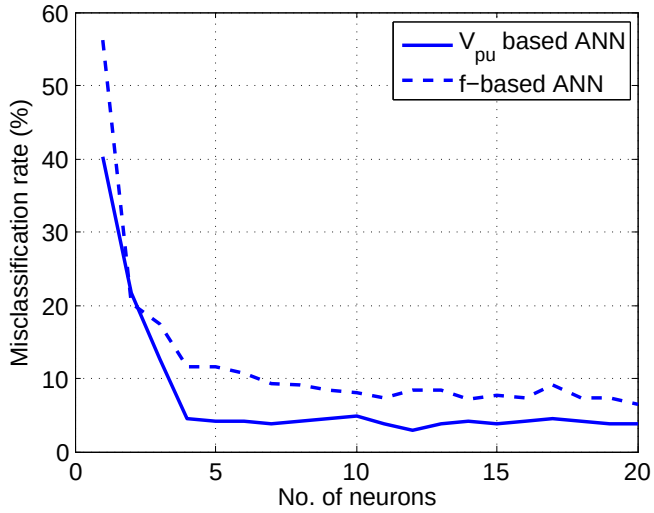

Figure 44. Change of misclassification rate for two different ANNs

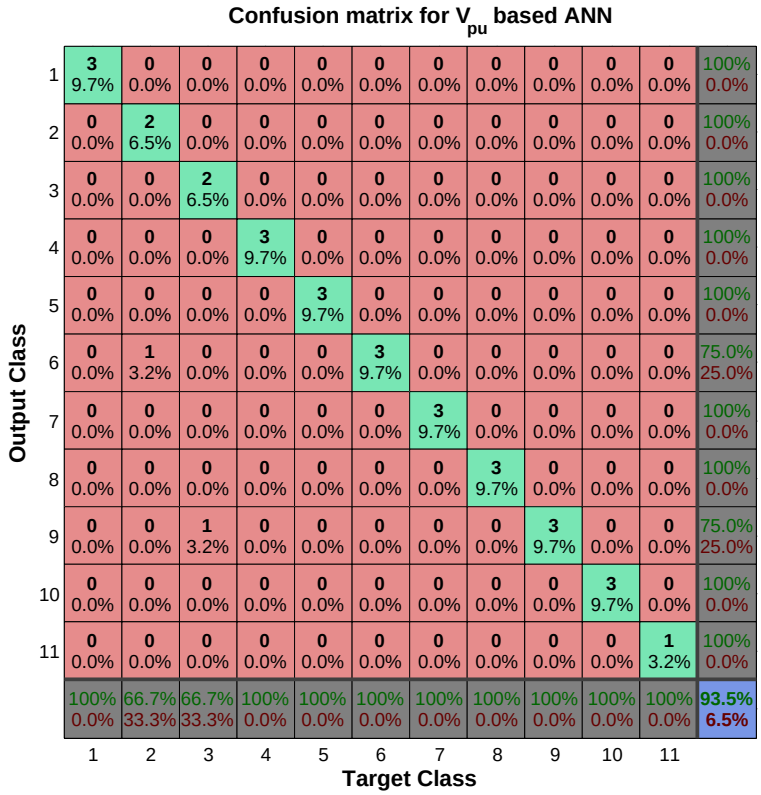

Figure 45. Confusion matrix for the optimized ANN trained with V_{pu} values

The misclassification rate shown is the average value after 10-fold cross-validation. It can be observed that the misclassification rate decreases drastically at first and then levels off. The selection of the number of neurons for each ANN is based on the smallest misclassification rate

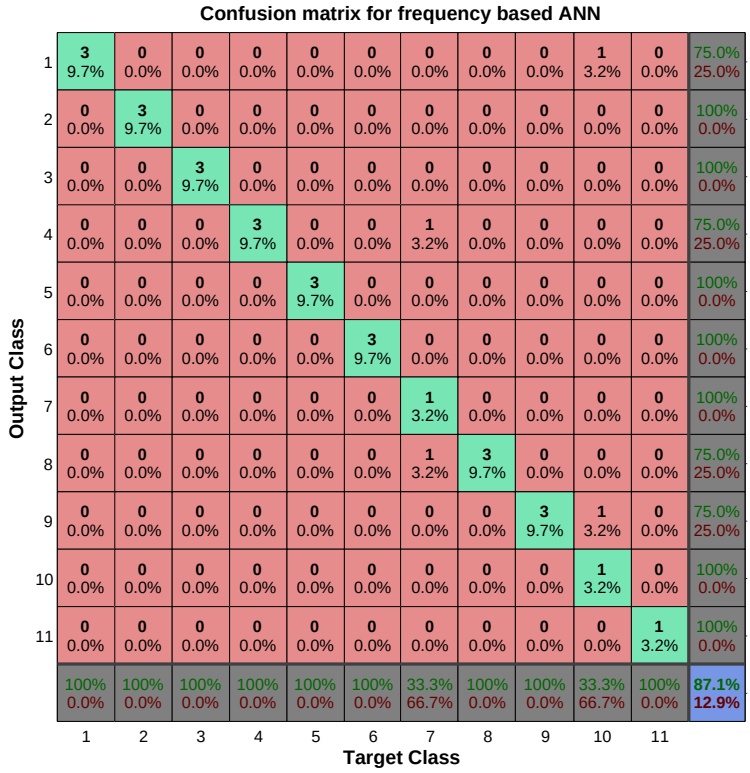

Figure 46. Confusion matrix for the optimized ANN trained with frequency values

observed. Table 13 lists, in descending order, the optimal neuron number of each ANN according to the corresponding classification accuracy.

Samples of confusion matrices for two different optimized ANNs are shown in figures 45 and 46. A confusion matrix provides details about the overall results of a classification test. It is a two-dimensional matrix having the output classes along the rows and the target classes along the columns. The green cells in the confusion matrices represent the number of correct classification results while the red ones repsresent the number of incorrect classifications. Therefore, from a confusion matrix, the percentage accuracy of each type of event can be determined. Furthermore, the matrix provides details into the actual versus predicted classification. This information can be used to identify which events cause the most confusion during classification. In each of the two confusion matrices, each class is an event. The numbering of the events are listed in table 14.

The lowest performing parameters were now eliminated one by one and the classification performance of the majority vote was observed at each step to reach an optimal combination of parameters for to implementing the event classification technique. Table 15 lists the performance of the technique at each step of the process.

Table 14. Event number and description in the confusion matrices

Event Number	**Event Description**
1	Capacitor closing
2	Capacitor opening
3	Line to line fault
4	Load switching
5	Loss of parallel feeder
6	Islanding condition with reactive mismatch
7	Islanding condition with real mismatch
8	Islanding condition with reactive mismatch
9	Islanding condition with real mismatch
10	Single line to ground fault
11	Three phase fault
12	Normal operation

Table 15. Classification accuracy in the majority vote for different combinations of ANNs

No. of Parameters	**Accuracy in Majority Vote (%)**	**Eliminated Parameter**
8	96.13	None
7	96.77	$\frac{dPF}{dt}$
6	96.77	PF
5	98.06	THD_I
4	96.45	THD_V
3	96.13	$\frac{dV}{dt}$

Table 16. Classification accuracy for each event

Event	**Classification accuracy(%)**
Reactive mismatch	99
Normal operation	99
Capacitor closing	99.66
Real mismatch	99.66
Capacitor opening	100
Line to line fault	100
Load closing	100
Load opening	100
Loss of parallel feeder	100
Single line to ground fault	100
3 phase fault	100

Figure 47 presents the structure of the optimized classification technique. It consists of 5 parametric ANNs and has a very high classification accuracy of 98.06%. Each ANN has only one

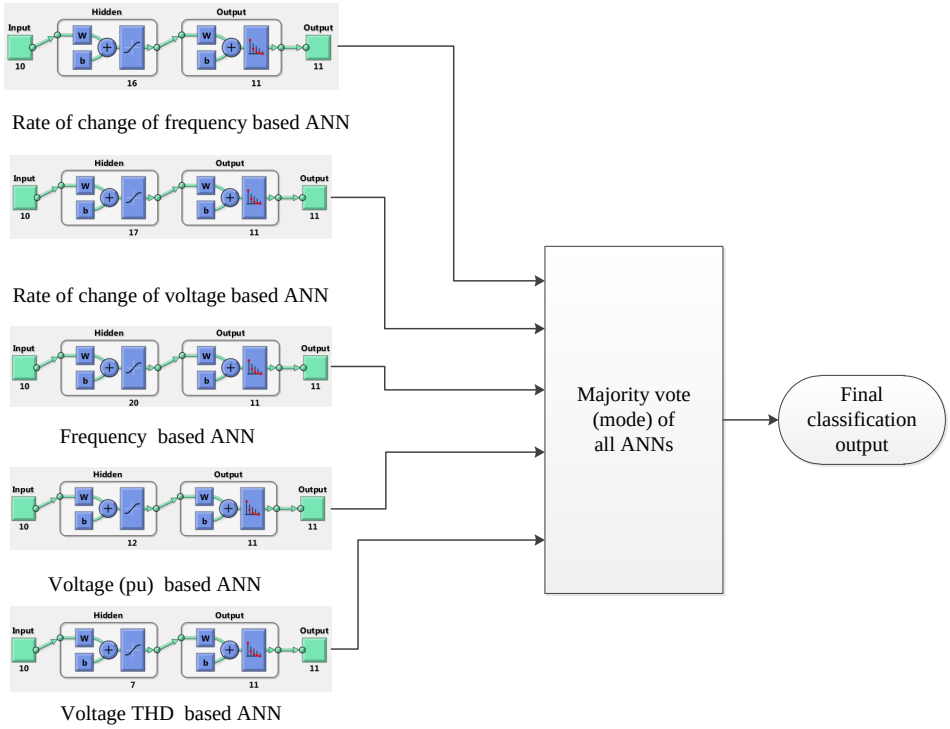

Figure 47. DG event classification technique block diagram

hidden layer and one output layer. The number of neurons in each hidden layer varied because they were selected according to optimal performance. The number of neurons in each output layer is the same and is equal to the number of classes. The overall classification performance of the model with respect to each type of event is listed in table 16. It can be observed that most of the events are classified without any error, and the error rate for the remaining ones is very low ($< 1\%$).

Chapter 5

CONCLUSIONS AND FUTURE WORK

This thesis proposed two novel passive islanding detection techniques and a unique event classification technique for smart DG systems. The islanding detection techniques monitor, in time domain, the ripple content in the RMS voltage and rate of change of frequency respectively. Islanding is detected if the ripple content is higher than a predefined threshold for a certain period of time. The proposed techniques were extensively tested with a variety of possible islanding scenarios, including active and reactive power mismatches over a wide range with RLC loads of varying quality factor. The tested non-islanding scenarios included faults, loss of parallel feeder, load switching, capacitor bank switching and motor starting. The techniques successfully detected islanding even for the worst case scenario of zero percent power mismatch. Furthermore, they accurately distinguished islanding events from the tested non-islanding events. The presence of dynamic loads such as motors had no significant impact on the performance of the technique. Furthermore, the techniques are independent of the nominal settings of the DG. The voltage RMS-based technique detects islanding within 300 ms while the rate of change of frequency based technique detects within 400 ms. Both of these detection times are well below the 2 s imposed by the IEEE 1547 standards. In addition, both techniques are computationally inexpensive and can be easily implemented into a PV inverter. Future work in this topic will consist of validating the techniques experimentally and also investigating the technique's performance in a large and complicated power system.

The proposed event classification technique is able to detect and classify local events which have considerable impact on the safety and operation of such DG systems. This technique is implemented using the pattern recognition feature of ANNs. Five parallel ANNs were used for classification. Each neural network was optimally designed to classify based on a specific local parameter. The output of each neural network is then arranged in a vector and the majority vote of the five is selected as the final classification output. A total of 310 sample cases of islanded and grid-connected events were generated to test the performance of the technique. The accuracy of the proposed event classification technique was verified using 10-fold cross-validation. The technique classified the event within 10 cycles of event occurrence with over 98% average classification accuracy. The implementation of such a classification feature in distributed generation systems will help the system operator develop a clear understanding of the operating characteristics to mitigate the effects of such events. Furthermore, the technique can classify an islanding event according to the type of mismatch within

the island. This capability can help the system make informed actions to react to these events after islanding. The performance of this technique in a more complicated microgrid will be investigated in the future.

Bibliography

Abd-Elkader, A, D. Allam, and E. Tageldin. 2014. Islanding detection method for DFIG wind turbines using artificial neural networks. *International Journal of Electrical Power and Energy Systems* 62:335–343.

Ackermann, T., G. Andersson, and L. Söder. 2001. Distributed generation: a definition. *Electric Power Systems Research* 57 (3): 195–204.

Aggarwal, R., and Y. Song. 1998. Artificial neural networks in power systems. III. Examples of applications in power systems. *Power Engineering Journal* 12, no. 6 (December): 279–287.

Akhlaghi, S., A. Ghadimi, and A. Akhlaghi. 2014. A novel hybrid islanding detection method combination of SMS and Q-f for islanding detection of inverter- based DG. In *Power and Energy Conference at Illinois (PECI),* 1–8. February.

El-Arroudi, K., G. Joos, I Kamwa, and D. McGillis. 2007. Intelligent-based approach to islanding detection in distributed generation. *IEEE Transactions on Power Delivery* 22, no. 2 (April): 828–835.

Asiminoaei, L., R. Teodorescu, F. Blaabjerg, and U. Borup. 2005. A digital controlled pv-inverter with grid impedance estimation for ens detection. *IEEE Transactions on Power Electronics* 20, no. 6 (November): 1480–1490.

Basu, J., D. Bhattacharyya, and T. Kim. 2010. Use of artificial neural network in pattern recognition. *International journal of software engineering and its applications* 4 (2).

Bayod-Rújula, A. 2009. Future development of the electricity systems with distributed generation. 6th World Energy System Conference on Advances in Energy Studies, *Energy* 34 (3): 377–383.

Bower, I., and M. Ropp. 2002. Evaluation of islanding detection methods for utility-interactive inverters in photovoltaic systems. *Sandia Laboratories.*

Cai, W., B. Liu, S. Duan, and C. Zou. 2013. An islanding detection method based on dual-frequency harmonic current injection under grid impedance unbalanced condition. *IEEE Transactions on Industrial Informatics* 9, no. 2 (May): 1178–1187.

Chang, W. 2010. A hybrid islanding detection method for distributed synchronous generators. In *International Power Electronics Conference (IPEC).* June.

Chen, Y., L. Le Xie, and P. Kumar. 2014. Power system event classification via dimensionality reduction of synchrophasor data. In *IEEE 8th Sensor Array and Multichannel Signal Processing Workshop,* 57–60. June.

Chilukuri, M., P. Dash, and K. Basu. 2004. Time-frequency based pattern recognition technique for detection and classification of power quality disturbances. In *IEEE Region 10 Conference (TENCON),* 3:260–263. November.

Crowhurst, B., E.F. El-Saadany, L. El Chaar, and L.A. Lamont. 2010. Single-phase grid-tie inverter control using dq transform for active and reactive load power compensation. In *IEEE International Conference on Power and Energy (PECon),* 489–494. November.

DOE. 2013. Economic benefits of increasing electric grid resilience to weather outages. *US President's Council of Economic Advisers and the U.S. Department of Energy's Office of Electricity Delivery and Energy Reliability.* http://energy.gov/sites/prod/files/2013/08/f2/Grid%20Resiliency%20Report_FINAL.pdf.

Dong, X., Y. Lu, and Y. Yang. 2009. A C4.5-based research on islanding detection in distributed generation system. In *8th International Conference on Advances in Power System Control, Operation and Management (APSCOM),* 1–7. November.

Eristi, H., and Y. Demir. 2012. Classification of power quality events and disturbances using wavelet transform and support vector machines. *IET Generation, Transmission, and Distribution* 6, no. 10 (October): 968–976.

Estebanez, E., V. Moreno, A. Pigazo, M. Liserre, and A. DellAquila. 2011. Performance Evaluation of Active Islanding-Detection Algorithms in Distributed-Generation Photovoltaic Systems: Two Inverters Case. *IEEE Transactions on Industrial Electronics* 58, no. 4 (April): 1185–1193.

Faqhruldin, O., E. El-Saadany, and H. Zeineldin. 2014. A universal islanding detection technique for distributed generation using pattern recognition. *IEEE Transactions on Smart Grid* 5, no. 4 (July): 1985–1992.

Fayyad, Y., and A. Osman. 2010. Neuro-wavelet based islanding detection technique. In *IEEE Electric Power and Energy Conference,* 1–6. August.

Freitas, W., and W. Xu. 2004. False operation of vector surge relays. *IEEE Transactions on Power Delivery* 19, no. 1 (January): 436–438.

Gupta, P., R. Bhatia, and D. Jain. 2015. Average absolute frequency deviation value based active islanding detection technique. *IEEE Transactions on Smart Grid* 6, no. 1 (January): 26–35.

Heeter, J., and T. Nicholas. 2013. Status and Trends in the U.S. Voluntary Green Power Market. *National Renewable Energy Laboratory.* http://energy.gov/sites/prod/files/2013/08/f2/Grid%20Resiliency%20Report_FINAL.pdf.

Hernandez-Gonzalez, G., and R. Iravani. 2006. Current injection for active islanding detection of electronically-interfaced distributed resources. *IEEE Transactions on Power Delivery* 21, no. 3 (July): 1698–1705.

Hines, P., J. Apt, and S. Talukdar. 2009. Large blackouts in North America: Historical trends and policy implications. *Energy Policy* 37 (12): 5249–5259.

IEC62116. 2009. International standard test procedure for utility-interconnected photovoltaic inverters.

IEEE1159. 2009. IEEE Recommended Practice for Monitoring Electric Power Quality (June).

IEEE1547. 2009. IEEE Application Guide for IEEE Std 1547(TM), IEEE Standard for Interconnecting Distributed Resources with Electric Power Systems (April).

Isa, I., S. Omar, Z. Saad, and M. Osman. 2010. Performance comparison of different multilayer perceptron network activation functions in automated weather classification. In *Fourth Asia International Conference on Mathematical/Analytical Modelling and Computer Simulation,* 71–75. May.

Jang, S., and K. Kim. 2004. An islanding detection method for distributed generations using voltage unbalance and total harmonic distortion of current. *IEEE Transactions on Power Delivery* 19, no. 2 (April): 745–752.

Jeraputra, C., and P. Enjeti. 2004. Development of a robust anti-islanding algorithm for utility interconnection of distributed fuel cell powered generation. *IEEE Transactions on Power Electronics* 19, no. 5 (September): 1163–1170.

Khamis, A., H. Shareef, E. Bizkevelci, and T. Khatib. 2013. A review of islanding detection techniques for renewable distributed generation systems. *Renewable and Sustainable Energy Reviews* 28:483–493.

Laaksonen, H. 2013. Advanced islanding detection functionality for future electricity distribution networks. *IEEE Transactions on Power Delivery* 28, no. 4 (October): 2056–2064.

Laghari, J., H. Mokhlis, H. Bakar, and M. Karimi. 2013. A new islanding detection technique for multiple mini hydro based on rate of change of reactive power and load connecting strategy. *Energy Conversion and Management* 76:215–224.

Laghari, J., H. Mokhlis, M. Karimi, A. Bakar, and H. Mohamad. 2014. Computational intelligence based techniques for islanding detection of distributed generation in distribution network: a review. *Energy Conversion and Management* 88:139–152.

Lidula, N., N. Perera, and A. Rajapakse. 2009. Investigation of a fast islanding detection methodology using transient signals. In *IEEE Power Energy Society General Meeting,* 1–6. July.

Mahat, P., Z. Chen, and B. Bak-Jensen. 2008. Review of islanding detection methods for distributed generation. In *Third international conference on electric utility deregulation and restructuring and power technologies,* 2743–2748. April.

Mahela, O., A. Shaik, and N. Gupta. 2015. A critical review of detection and classification of power quality events. *Renewable and Sustainable Energy Reviews* 41:495–505.

Massoud, A., K. Ahmed, S. Finney, and B. Williams. 2009. Harmonic distortion-based island detection technique for inverter-based distributed generation. *IET Renewable Power Generation* 3:493–507.

Matic-Cuka, B., and M. Kezunovic. 2014. Islanding detection for inverter-based distributed generation using support vector machine method. *IEEE Transactions on Smart Grid* 5, no. 6 (November): 2676–2686.

Menon, V., and M. Nehrir. 2007. A hybrid islanding detection technique using voltage unbalance and frequency set point. *IEEE Transactions on Power Systems* 22, no. 1 (February): 442–448.

Miller, C. E. 1952. Voltage rating versus horsepower of synchronous and induction motors. *Transactions of the American Institute of Electrical Engineers, Part II: Applications and Industry,* 71, no. 5 (November): 306–311.

Moeini, A., A. Ahmad Darabi, S. Rafiei, and M. Karimi. 2011. Intelligent islanding detection of a synchronous distributed generation using governor signal clustering. *Electric Power Systems Research* 81:608–616.

Moller, M. 1993. A scaled conjugate gradient algorithm for fast supervised learning. *Neural networks* 6 (4): 525–533.

Najy, W., H. Zeineldin, A. Alaboudy, and W. Woon. 2011. A Bayesian Passive Islanding Detection Method for Inverter-Based Distributed Generation Using ESPRIT. *IEEE Transactions on Power Delivery* 26, no. 4 (October): 2687–2696.

Pai, F., and S. Huang. 2001. A detection algorithm for islanding-prevention of dispersed consumer-owned storage and generating units. *IEEE Transactions on Energy Conversion* 16, no. 4 (December): 346–351.

Pena, P., A. Etxegarai, L. Valverde, I. Zamora, and R. Cimadevilla. 2013. Synchrophasor-based anti-islanding detection. In *IEEE Grenoble PowerTech,* 1–6. June.

Ray, P., S. Mohanty, and N. Kishor. 2013. Classification of power quality disturbances due to environmental characteristics in distributed generation system. *IEEE Transactions on Sustainable Energy* 4, no. 2 (April): 302–313.

Reaz, M., F. Choong, M. Sulaiman, F. Mohd-Yasin, and M. Kamada. 2007. Expert system for power quality disturbance classifier. *IEEE Transactions on Power Delivery* 22, no. 3 (July): 1979–1988.

REN21. 2014. Renewables 2014 global status report. http://www.ren21.net/Portals/0/documents/Resources/GSR/2014/GSR2014_full%20report_low%20res.pdf.

Ropp, M., K. Aaker, J. Haigh, and N. Sabbah. 2000. Using power line carrier communications to prevent islanding of PV power systems. In *Twenty-Eighth IEEE Photovoltaic Specialists Conference,* 1675–1678.

Ropp, M.E., M. Begovic, and A. Rohatgi. 1999. Analysis and performance assessment of the active frequency drift method of islanding prevention. *IEEE Transactions on Energy Conversion* 14, no. 3 (September): 810–816.

Ruqiang, Y., and R. Gao. 2009. Tutorial 21 wavelet transform: a mathematical tool for non-stationary signal processing in measurement science part 2 in a series of tutorials in instrumentation and measurement. *IEEE Instrumentation Measurement Magazine* 12, no. 5 (October): 35–44.

Saini, M., and R. Kapoor. 2012. Classification of power quality events – a review. *International Journal of Electrical Power and Energy Systems* 43 (1): 11–19.

Salman, S., D. King, and G. Weller. 2004. Investigation into the development of a new ANN-based relay for detecting loss of mains of embedded generation. In *Eighth IEEE International Conference on Developments in Power System Protection,* vol. 2, 579–582 Vol.2. April.

Samantaray, S.R. 2010. Decision tree-initialised fuzzy rule-based approach for power quality events classification. *IET Generation, Transmission, and Distribution* 4, no. 4 (April): 530–537.

Stevens, J., R. Bonn, J. Ginn., S. Gonzalez, and G. Kern. 2000. Development and testing of an approach to anti-islanding in utility-interconnected photovoltaic systems. *Sandia National Laboratories.*

Sykes, J., K. Koellner, W. Premerlani, B. Kasztenny, and M. Adamiak. 2007. Synchrophasors: a primer and practical applications. In *Power systems conference on advanced metering, protection, control, communication, and distributed resources,* 213–240. March.

Tedde, M., and K. Smedley. 2014. Anti-islanding for three-phase one-cycle control grid tied inverter. *IEEE Transactions on Power Electronics* 29, no. 7 (July): 3330–3345.

UL1741. 2001. UL Standard for Safety for Static Converters and Charge Controllers for Use in Photovoltaic Power Systems. *Underwriters Laboratories.*

Valtierra-Rodriguez, M., R. de Jesus Romero-Troncoso, R.A. Osornio-Rios, and A. Garcia-Perez. 2014. Detection and classification of single and combined power quality disturbances using neural networks. *IEEE Transactions on Industrial Electronics* 61, no. 5 (May): 2473–2482.

Walling, R.A., and N.W. Miller. 2002. Distributed generation islanding-implications on power system dynamic performance. In *IEEE Power Engineering Society Summer Meeting,* vol. 1, 92–96 vol.1. July.

Wang, W., J. Kliber, G. Zhang, W. Xu, B. Howell, and T. Palladino. 2007. A Power Line Signaling Based Scheme for Anti-Islanding Protection of Distributed Generators - Part II: Field Test Results. *IEEE Transactions on Power Delivery* 22, no. 3 (July): 1767–1772.

Wilsun Xu, W., G. Zhang, C. Li, W. Wang, G. Wang, and J. Kliber. 2007. A Power Line Signaling Based Technique for Anti-Islanding Protection of Distributed Generators - Part I: Scheme and Analysis. *IEEE Transactions on Power Delivery* 22, no. 3 (July): 1758–1766.

Zhihong, Y., A. Kolwalkar, Y. Zhang, Pengwei Du, and R. Walling. 2004. Evaluation of anti-islanding schemes based on nondetection zone concept. *IEEE Transactions on Power Electronics* 19, no. 5 (September): 1171–1176.